ANNUAL REVIEWS

Annual Review of Condensed Matter Physics Quantum Many-Body Scars: A Quasiparticle Perspective

Anushya Chandran,¹ Thomas Iadecola,^{2,3} Vedika Khemani,⁴ and Roderich Moessner⁵

- ¹Department of Physics, Boston University, Boston, Massachusetts, USA; email: anushyac@bu.edu
- ²Department of Physics and Astronomy, Iowa State University, Ames, Iowa, USA
- ³Ames Laboratory, Ames, Iowa, USA
- ⁴Department of Physics, Stanford University, Stanford, California, USA
- ⁵Max-Planck-Institut für Physik komplexer Systeme, Dresden, Germany



www.annualreviews.org

- · Download figures
- Navigate cited references
- Keyword search
- · Explore related articles
- Share via email or social media

Annu. Rev. Condens. Matter Phys. 2023. 14:443-69

First published as a Review in Advance on December 21, 2022

The Annual Review of Condensed Matter Physics is online at commatphys.annualreviews.org

https://doi.org/10.1146/annurev-conmatphys-031620-101617

Copyright © 2023 by the author(s). This work is licensed under a Creative Commons Attribution 4.0 International License, which permits unrestricted use, distribution, and reproduction in any medium, provided the original author and source are credited. See credit lines of images or other third-party material in this article for license information.



Keywords

eigenstate thermalization, quantum chaos, out-of-equilibrium quantum dynamics, constrained dynamics

Abstract

Weakly interacting quasiparticles play a central role in the low-energy description of many phases of quantum matter. At higher energies, however, quasiparticles cease to be well defined in generic many-body systems owing to a proliferation of decay channels. In this review, we discuss the phenomenon of quantum many-body scars, which can give rise to certain species of stable quasiparticles throughout the energy spectrum. This goes along with a set of unusual nonequilibrium phenomena including many-body revivals and nonthermal stationary states. We provide a pedagogical exposition of this physics via a simple yet comprehensive example, that of a spin-1 XY model. We place our discussion in the broader context of symmetry-based constructions of many-body scar states, projector embeddings, and Hilbert space fragmentation. We conclude with a summary of experimental progress and theoretical puzzles.

1. INTRODUCTION

Interacting quantum matter can exhibit excitations—e.g., phonons in solids or magnons in magnets—that involve the collective motion of many particles and yet, remarkably, act like a single emergent entity. Such objects are dubbed quasiparticles. The emergence of long-lived quasiparticles in very different types of condensed matter systems is so commonplace that one barely registers just how remarkable a phenomenon it is.

There are various well-established mechanisms for stabilizing quasiparticles at low energies as encoded, for instance, in Goldstone's theorem for broken continuous symmetries, or in Ginzburg's kinematic argument for long-lived quasielectrons and quasiholes in Fermi liquids (1–3). In contrast, stabilizing quasiparticles at higher energies is a different issue altogether. It is commonly believed that quasiparticles become unstable when they encounter the continuum of many-particle excited states at high energies and decay swiftly when kinematically permitted.

The existence of long-lived quasiparticles at energies well above the single-quasiparticle bandwidth should therefore register surprise. In fact, there exist various routes toward stabilizing quasiparticles beyond the low-energy limit. Perhaps the most straightforward of these arises in the case of noninteracting particles, where long lifetimes arise owing to the complete absence of decay processes. This comprises rather important phenomena such as Anderson localization as well as any noninteracting—e.g., topological—band structures, and includes spin systems related to such models via Jordan–Wigner transformations. More elaborate are interacting integrable models, such as low-dimensional models soluble by the Bethe ansatz (4–7), where particles scatter without decaying. The presence of certain symmetries can also guarantee the existence of infinitely long-lived quasiparticles, as in the η -pairing eigenstates of the Fermi–Hubbard model (8). Furthermore, sufficiently strong interactions may actually impede, rather than promote, quasiparticle decay in certain energy windows (9–11).

The subject of this review concerns a new mechanism for obtaining stable quasiparticles in interacting systems, which goes under the heading of "quantum many-body scars." This term was coined in Reference 12 by analogy to the phenomenon of wave function scarring in singleparticle quantum mechanical systems arising from the quantization of a corresponding classical model (13). In such systems, quantum mechanical wave functions exhibit regions of enhanced probability, called scars, concentrated around unstable periodic trajectories of the classical system. The analogy posited in Reference 12 defines quantum many-body scars as the existence of special highly-excited eigenstates with atypically large weights on certain simple many-body states. The dynamics of the many-body system, when prepared in one of these simple states, becomes strongly nonthermal. For example, the system can exhibit finite-time revivals of the many-body wave function, which generically occurs only at astronomically long times (associated with Poincaré recurrence) in nonintegrable systems (14). Although a variety of mechanisms for quantum manybody scars have been proposed, a ubiquitous one is the emergence of a small subset of stable quasiparticles, out of which special many-particle states throughout the many-body spectrum can be constructed (15–29). In idealized models, such quasiparticles have infinite lifetime, in contrast to the naive expectation outlined above.

These phenomena represent a deviation from the expected behavior of generic (i.e., interacting, nonintegrable) quantum many-body systems. The coherent quantum many-body dynamics of such systems has been the subject of a separate thread of investigation of much current interest. Nucleated by experimental developments—e.g., the advent of analog and digital quantum simulation platforms with low levels of environmental decoherence (30–33)—one important question has been the connection between microscopic quantum theory and macroscopic thermodynamics (34, 35). The eigenstate thermalization hypothesis (ETH; 36–39) is a central concept in this

context. It states that an eigenstate, $|\alpha\rangle$, of a many-body Hamiltonian, $H|\alpha\rangle = E_{\alpha}|\alpha\rangle$, exhibits the same properties as the appropriate Gibbs ensemble at the energy density $\epsilon_{\alpha} = E_{\alpha}/V$ to leading order in the volume V of the system. For example, for any few-body operator O, the eigenstate expectation value $\langle \alpha|O|\alpha\rangle$ is a smooth function of ϵ_{α} . Similarly, if one partitions the system into two subregions A and B and calculates the reduced density matrix $\rho_{A} = \operatorname{tr}_{B}|\alpha\rangle\langle\alpha|$, the entanglement entropy $S_{A} = -\operatorname{tr}(\rho_{A}\ln\rho_{A})$ scales extensively with the volume of A at any finite temperature with the coefficient set by the thermal entropy density at the energy density ϵ_{α} . In other words, the exponentially large amount of microscopic information encoded in the coefficients of the wave function on Hilbert space appears to be largely superfluous when determining thermodynamic observables.

A many-body eigenstate in which expectation values of few-body observables differ from the thermodynamic values is thus at odds with eigenstate thermalization. In the aforementioned examples of noninteracting and interacting integrable systems, the ETH as stated above does not apply and must be generalized to account for an extensive number of additional conserved quantities (40). It is believed that the addition of a generic local perturbation of finite strength destroys the special features associated with integrability and gives way to conventional thermalizing behavior (41–45). The one generic exception to the ETH is believed to be provided by many-body localization (MBL) in strongly disordered yet interacting systems (46, 47), in which extensively many local conserved degrees of freedom preclude thermalization (48–50). However, the existence of such stable emergent integrability is still being debated (51–56).

Unlike systems with explicit or emergent integrability, systems with quantum many-body scars exhibit features that contrast with the ETH, but only in a fraction of (excited) states that vanish in the thermodynamic limit. The vast majority of eigenstates instead look thermal. The nonthermal features may be broadly classified into the following three categories:

- 1. the existence of certain species of infinitely long-lived quasiparticles,
- 2. persistent many-body revivals at finite times in the dynamics, and
- nonthermal stationary states (e.g., eigenstates or late-time states under time evolution) that have atypically low (i.e., subthermal) entanglement and large weights on certain simple states.

All of these features signal an absence of thermalization, touching on different aspects of the phenomenon. We reiterate that these nonthermal features are found in special states sprinkled throughout the many-body spectrum—i.e., at all temperatures, including infinite temperature—and these special states coexist with typical thermal states at the same energy densities. The nomenclature of scarring has variously been used in the literature to signify the presence of any one of the above categories or of all three at the same time. In this review, we discuss quantum many-body scars from a quasiparticle perspective, and draw comparisons and contrasts with other perspectives on scarring and related phenomena. Two other recent reviews on quantum many-body scars provide complementary perspectives to this one. The first, Reference 57, highlights the connections to classical periodic orbits using semiclassics, whereas the second, Reference 58, presents various exact results and matrix product state—based understanding.

The remainder of this review is organized as follows: For pedagogical simplicity and clarity, we introduce quantum many-body scars in Section 2.1 via a particularly simple model that exhibits the above nonthermal categories 1–3 in a physically transparent way. We then discuss quasiparticle-based many-body scarring more generally, focusing on a descriptive formalism in Section 2.2 and constructive principles for building models with scars in Section 2.3. In Section 3, we explore other perspectives on scarring with the same emphasis on descriptive and constructive

approaches. Finally, in Section 4, we describe experimental observations of quantum many-body scars in various systems. We especially focus on the original experimental observation of scarring in a Rydberg system presented in Reference 59 and highlight theoretical attempts to explain this experiment via studies of the so-called PXP model and its deformations; again, we focus on various manifestations of quasiparticles in these different accounts.

2. QUANTUM SCARS FROM STABLE QUASIPARTICLES

2.1. An Illustrative Solvable Example

In this section, we show how the three phenomena characteristic of quantum scarring emerge in a simple model, the spin-1 XY model. We focus on this model for pedagogical clarity but note that the phenomenon of quasiparticles emerging at finite energy density in a nonintegrable model was first predicted in References 15 and 16 for the Affleck–Kennedy–Lieb–Tasaki (AKLT) chain (60).

We follow the approach in Reference 17 and discuss a one-dimensional version of the model to simplify the presentation. However, many of the properties hold on the *d*-dimensional hypercubic lattice or indeed any bipartite graph. The model is given by

$$H = JH_{XY} + b S^{z}$$

$$= J \sum_{r} (S_{r}^{x} S_{r+1}^{x} + S_{r}^{y} S_{r+1}^{y}) + b \sum_{r} S_{r}^{z},$$
1.

where r = 1, ..., L labels lattice sites. The operators S_r^{α} ($\alpha = x, y, z$) are spin-1 operators, and we choose a local basis $|\pm_r\rangle$, $|0_r\rangle$ whose eigenvalues under S_r^z are ± 1 and 0, respectively. The model in Equation 1 is nonintegrable, even in one dimension, and therefore is expected to obey the ETH upon resolving all microscopic symmetries. This can be shown numerically by computing, e.g., the statistics of spacings between neighboring energy levels (61; see **Figure 1a**). Nevertheless, the model supports a tower of exact many-body eigenstates with a simple structure and atypical properties relative to other eigenstates at the same energy density. These scarred eigenstates have an appealing interpretation in terms of many-particle states of bimagnon quasiparticles (i.e., bound states of two magnons), whose scattering and decay are inhibited by a destructive interference effect that is absent for other quasiparticle types, e.g., single magnons.

2.1.1. Exact (nonscarred) eigenstates dictated by symmetry. The model in Equation 1 has two bands of exact single-magnon states in its spectrum owing to a symmetry. To see this, note that the polarized states $|\Omega\rangle = \bigotimes_{r=1}^{L} |-_r\rangle$ and $|\Omega'\rangle = \bigotimes_{r=1}^{L} |+_r\rangle$ are annihilated by H_{XY} . Single-magnon states can be built atop these polarized states using the spin raising and lowering operators $S_r^{\pm} = S_r^{\times} \pm i S_r^{y}$:

$$|+,k\rangle = \frac{1}{\sqrt{2L}} \sum_{r=1}^{L} e^{ikr} S_r^+ |\Omega\rangle,$$
 2a.

$$|-,k\rangle = \frac{1}{\sqrt{2L}} \sum_{r=1}^{L} e^{ikr} S_r^- |\Omega'\rangle,$$
 2b.

where $k = \frac{2\pi}{L} p$ (p = 0, ..., L - 1). These single-magnon states have energies $E_{\pm,k} = \mp b(L-1) + 2J \cos k$. Their existence is guaranteed by the U(1) symmetry $[H, S^z] = 0$, and by translation invariance. Indeed, the polarized states $|\Omega\rangle$ and $|\Omega'\rangle$ must be eigenstates of H because they are the unique states with $S^z = \pm L$. There are 2L spin configurations with $S^z = \pm (L-1)$; translation invariance organizes these states into the single-magnon plane waves of Equation 2, and

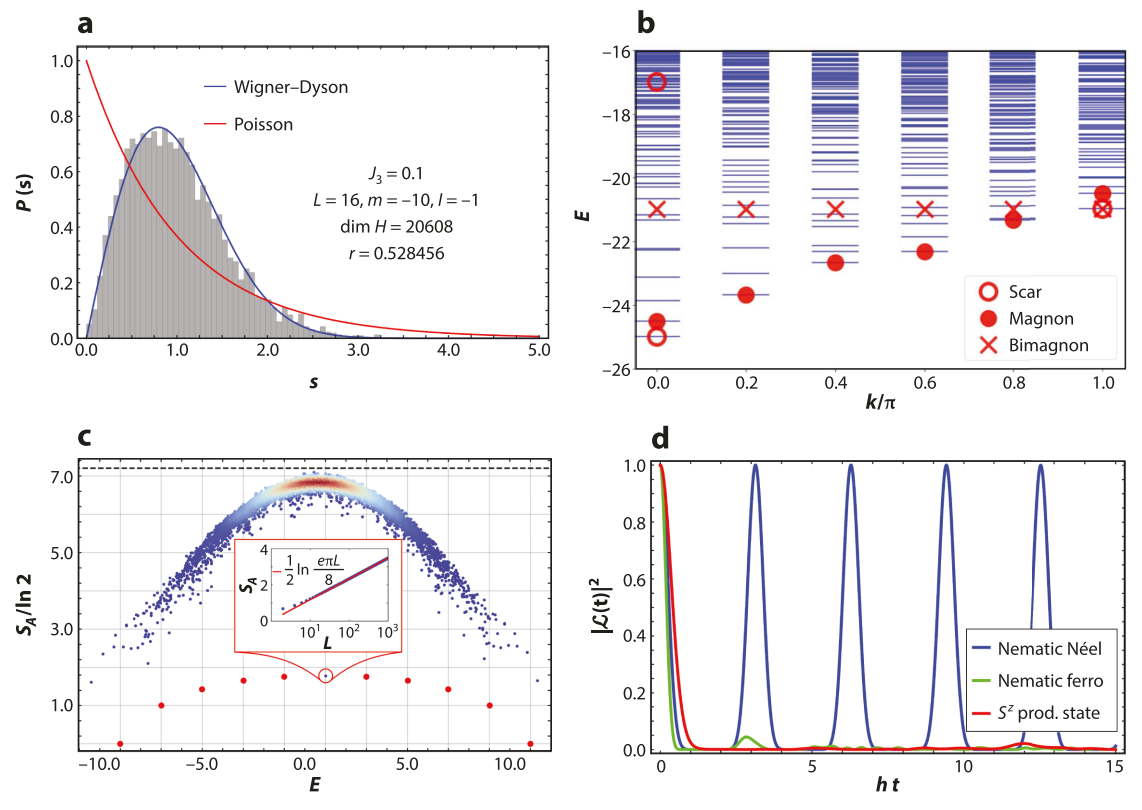


Figure 1

Scars in the spin-1 XY model. (a) Distribution P(s) of nearest-neighbor energy level spacings s for the model defined in Equation 1 in the presence of third-neighbor hopping terms (Equation 17). The energy-level spacings follow a Wigner-Dyson distribution (blue curve), a strong indicator of nonintegrability. (b) Low-energy spectrum of the spin-1 XY model as a function of momentum k, with L=10 and parameters chosen such that the polarized state $|\Omega\rangle$ is the ground state. The scar states $|S_n\rangle$ for n=0,1, and 2 are marked with empty red circles, whereas the single-magnon states described in Section 2.1.1 are marked with filled red circles. Red crosses denote the energy expectation values of single bimagnon states for different values of k; only the one with $k=\pi$ is an exact eigenstate. (c) Half-chain entanglement entropy S_A as a function of energy in the zero-magnetization sector for a chain with L=10 sites. The scar state in the zero magnetization sector is circled in red, and the inset demonstrates that the entanglement entropy of this state scales logarithmically with L. The entanglement entropies of the scar states in other magnetization sectors are denoted by red points. The dashed line denotes the value of the entanglement entropy for a random state, which obeys volume-law scaling (see 62). (d) Dynamics of the Loschmidt echo, Equation 14, for the initial state, Equation 15 (blue), and L=8. The dynamics for two other initial product states (green, red) are shown for comparison. Panels a, c, and d adapted from Reference 17.

Figure 1b plots the low-energy spectrum of Equation 1 with an added third-neighbor exchange term (see Equation 17) as a function of quasimomentum k, with parameters chosen such that the fully polarized state $|\Omega\rangle$ is the ground state. The exact single-magnon eigenstates $|k,\Omega\rangle$ with $k=0,\ldots,\pi$ are also represented.

Symmetry alone is not sufficient to guarantee the existence of eigenstates with more than one magnon. Indeed, one readily finds that inserting additional magnons via multiple application of the operators $S_k^{\pm} = \sum_r e^{ikr} S_r^{\pm}$ does not yield exact eigenstates. (This can be seen, e.g., by calculating the energy variance of these multimagnon states.) Physically, this arises because multimagnon states are unstable to interaction effects (i.e., scattering processes) that open up various decay channels. Thus, other effects must conspire to stabilize eigenstates with additional quasiparticles.

2.1.2. Bimagnon tower of scar states. We now show that Equation 1 admits a tower of exact bimagnon states,

$$|S_n\rangle = \mathcal{N}(n)(J^+)^n |\Omega\rangle,$$
 3.

where n = 0, ..., L, $\mathcal{N}(n) = \sqrt{\frac{(L-n)!}{n!L!}}$ ensures normalization, and

$$J^{\pm} = \frac{1}{2} \sum_{r=1}^{L} e^{i\pi r} (S_r^{\pm})^2.$$
 4.

The operator J^+ inserts a bimagnon with momentum π into the vacuum $|\Omega\rangle$. The lowest-lying bimagnon state $|\mathcal{S}_1\rangle$ is marked at $k=\pi$ in **Figure 1b**, as are the polarized state $|\mathcal{S}_0\rangle = |\Omega\rangle$ and the state $|\mathcal{S}_2\rangle$. Single-bimagnon states at other momenta can also be constructed, and their energy expectation values are marked in the same figure. However, these single-bimagnon states are not generically eigenstates for $k \neq \pi$.

The infinite lifetime of bimagnon excitations at momentum π can be understood relatively simply. Consider the one-bimagnon state, which we rewrite as

$$|\mathcal{S}_1\rangle \propto \sum_{r=1}^{L} (-1)^r |\cdots - +_r - \ldots\rangle,$$
 5.

where we suppress the site indices away from site r for compactness. Observe that the local XY exchange term $b_{r,r+1}^{XY} = S_r^x S_{r+1}^x + S_r^y S_{r+1}^y$ acts as

$$b_{r,r+1}^{\rm XY} \left| -- \right\rangle = b_{r,r+1}^{\rm XY} \left| ++ \right\rangle = 0,$$
 6a.

$$b_{r,r+1}^{\rm XY}\left|+-\right\rangle = b_{r,r+1}^{\rm XY}\left|-+\right\rangle = \left|00\right\rangle. \tag{6b}.$$

Equation 6b indicates that the XY exchange term dissociates the bimagnon excitation into two magnons. From Equation 6, we deduce that $b_{r,r+1}^{XY}$ annihilates $|S_1\rangle$ for all r:

$$b_{r,r+1}^{XY} | \mathcal{S}_1 \rangle \propto b_{r,r+1}^{XY} | \cdots +_r - \ldots \rangle - b_{r,r+1}^{XY} | \cdots - +_{r+1} \ldots \rangle = 0.$$

This annihilation results from the destructive interference of the bimagnon dissociation processes $|+-\rangle \rightarrow |00\rangle$ and $|-+\rangle \rightarrow |00\rangle$, which arises owing to the alternating sign $e^{i\pi r}=(-1)^r$ in Equation 5. In fact, the above calculation can be applied to show that $b_{r,r+1}^{XY} | \mathcal{S}_n \rangle = 0$ for all n. Every spin configuration $|L\rangle \otimes |+-\rangle \otimes |R\rangle$ in $|\mathcal{S}_n\rangle$ has a partner configuration $|L\rangle \otimes |-+\rangle \otimes |R\rangle$ appearing with the opposite sign due to the fact that all of the bimagnons have momentum π . We therefore conclude that $H_{XY} | \mathcal{S}_n \rangle = 0$, so that $|\mathcal{S}_n\rangle$ are eigenstates of Equation 1 with energy $E_n = b(2n - L)$ set by the magnetic field.

An important feature of the states $|S_n\rangle$ is that they form a spin-L/2 representation of an SU(2) algebra generated by the raising and lowering operators J^{\pm} :

$$[J^+, J^-] = 2J^z, [J^z, J^{\pm}] = \pm J^{\pm},$$
 8.

where $J^z = \frac{1}{2} \sum_{r=1}^{L} S_r^z = \frac{1}{2} S^z$. Note that the states $|S_n\rangle$ are eigenstates of J^z , which is proportional to the magnetization operator S^z that couples to the magnetic field. Using the definition Equation 3 of the scar states, one can show that

$$\left[\frac{1}{2}(J^+J^- + \text{H.c.}) + (J^z)^2\right]|\mathcal{S}_n\rangle = j(j+1)|\mathcal{S}_n\rangle$$
 9a.

and

$$J^{\pm} | \mathcal{S}_n \rangle = \sqrt{j(j+1) - m(m\pm 1)} | \mathcal{S}_{n\pm 1} \rangle,$$
 9b.

where j = L/2 and m = n - L/2. The expressions in Equation 9 enable simple calculations of the expectation values of certain operators.

As might be anticipated from their simple structure (see Equation 3) and physical interpretation, the eigenstates $|S_n\rangle$ exhibit properties that are atypical of eigenstates nearby in energy. In particular, we should compare an eigenstate $|S_n\rangle$ with n/L finite as $L \to \infty$ to expectations based on the ETH, which governs typical eigenstates at the same energy density. One property that clearly demonstrates that the ETH does not hold in these eigenstates is the presence of off-diagonal long-range order (63), as witnessed by the correlation function

$$\frac{4}{L^2} \langle \mathcal{S}_n | J^- J^+ | \mathcal{S}_n \rangle = \left[1 - \frac{(2n-L)^2}{L^2} \right] + O\left(\frac{1}{L}\right).$$
 10.

This result is obtained by direct application of Equation 9. Notice that, unless n = 0 or L, the right-hand side of the above equation is finite in the thermodynamic limit. This means that the scarred eigenstates $|S_n\rangle$ contain long-range connected correlations (note that $\langle S_n|J^{\pm}|S_n\rangle = 0$). In contrast, for a generic eigenstate in the middle of the energy spectrum, the expected value of this correlation function based on ETH is given by the infinite-temperature average,

$$\frac{1}{3^L}\operatorname{tr}\left(\frac{4}{L^2}J^-J^+\right) = \frac{4}{3L},\tag{11}$$

which vanishes as $L \to \infty$. Another atypical feature of the eigenstates $|S_n\rangle$ is their entanglement entropy, which can be evaluated analytically using simple combinatorics (see Reference 17). The scaling with L of the entanglement entropy of the state $|S_{L/2}\rangle$ as $L \to \infty$ can be shown explicitly via saddle point arguments to be

$$\lim_{L \to \infty} S_A = \frac{1}{2} \left(\ln \frac{\pi L}{8} + 1 \right),\tag{12}$$

where $S_A = -\text{tr}(\rho_A \ln \rho_A)$, where $\rho_A = \text{tr}_B |S_{L/2}\rangle \langle S_{L/2}|$ and tr_B denotes the trace over sites 1, . . . , L/2. In contrast, the ETH predicts that finite-energy-density eigenstates of nonintegrable models like Equation 1 obey the volume-law scaling $S_A \sim L$. Numerical results emphasizing the weakly entangled nature of the scar states are shown in **Figure 1***c*.

Further evidence of the atypical nature of these eigenstates can be revealed by considering the dynamics from certain special initial states. In the presence of a finite magnetic field h, any state of the form

$$|\psi_0\rangle = \sum_{n=0}^{L} c_n |\mathcal{S}_n\rangle$$
 13.

experiences periodic revivals due to the equally spaced eigenenergies E_n . This is easiest to see in the so-called Loschmidt echo,

$$\mathcal{L}(t) = \langle \psi_0 | e^{-iHt} | \psi_0 \rangle = e^{ibLt} \sum_{n=0}^{L} |c_n|^2 e^{-in(2b)t}.$$
 14.

Up to an unimportant global phase, $\mathcal{L}(t)$ is a periodic function with period π/h . Numerical data exhibiting these periodic revivals are shown in **Figure 1***d*. This time-periodic behavior of the Loschmidt echo should be contrasted with the expectation for quantum chaotic systems, where a rapid decay is expected for typical initial states (64, 65). Remarkably, the family of initial states in

Equation 13 includes product states that are readily accessible experimentally. Perhaps the simplest of these is given by

$$|\phi_0\rangle = \bigotimes_r \left[\frac{|+_r\rangle - (-1)^r |-_r\rangle}{\sqrt{2}} \right],$$
 15.

which is of the form of Equation 13 with $c_n = (-1)^n \sqrt{\binom{L}{n} \frac{1}{2^L}}$. Physically, the state $|\phi_0\rangle$ corresponds to the ground state of the Hamiltonian

$$H_0 = \frac{1}{2}(J^+ + J^-)$$

$$= \frac{1}{2} \sum_{r=1}^{L} (-1)^r \left[(S_r^{\text{v}})^2 - (S_r^{\text{y}})^2 \right]$$
16.

formed from the quasiparticle creation and annihilation operators. H_0 is nothing but the generator J^x of the SU(2) algebra (Equation 8). As such, the periodic dynamics observed in Equation 14 can be interpreted as resulting from the precession of a macroscopic spin-L/2 object under the magnetic field term in Equation 1, which is proportional to J^z . This interpretation was put forward as an approximate description of the periodic dynamics in the PXP model in Reference 66 (see Section 4), but holds exactly in the case of the spin-1 XY model.

We conclude this section with a few comments regarding the model in Equation 1. First, we note that, in one dimension, the spin-1 XY model possesses a hidden nonlocal SU(2) symmetry when defined with open boundary conditions, and a twisted version thereof when defined with periodic boundary conditions (22, 67). Thus, confirming the nonintegrability of this model in one dimension requires resolving this additional unexpected symmetry. However, this symmetry is not essential to the presence of the scars in this model. For example, as noted in Reference 17, adding a third-neighbor XY exchange term of the form

$$H_3 = J_3 \sum_r (S_r^x S_{r+3}^x + S_r^y S_{r+3}^y)$$
 17.

breaks the hidden SU(2) symmetry while preserving the scar states. Indeed, one readily verifies that the destructive interference effect demonstrated in Equation 7 holds also for H_3 , the key commonality being that sites r and r+3 belong to opposite sublattices, as do sites r and r+1. In fact, this reasoning can be extended to show that any odd-neighbor XY exchange term preserves the scar tower. A variety of other terms can also be added to Equation 1 while preserving the tower of scar states. For example, in Reference 17 it was noted that the single-site anisotropy term $\sum_r (S_r^z)^2$ preserves the tower, because the states $|S_n\rangle$ are superpositions of tensor products of the local states $|\pm_r\rangle$, which satisfy $(S_r^z)^2 |\pm_r\rangle = |\pm_r\rangle$. Reference 20 presented a systematic enumeration of all nearest-neighbor terms that preserve the eigenstates $|S_n\rangle$.

2.2. Algebraic Descriptions

At a more abstract level, models with stable quasiparticles atop specific vacuum states have simple algebraic descriptions. There are three equivalent algebraic descriptions in the literature: spectrum-generating algebras (SGAs) (19, 21), quasisymmetry groups (26, 68), and group-invariant sectors (23–25). All three describe the scarred subspace using higher symmetries than those of the Hamiltonian itself, but they provide different constructive principles for the Hamiltonian and for the action of the symmetry on the scarred subspace (see Section 2.3). The scar towers in the spin-1 XY chain discussed above, generalized Hubbard models with η -pairing states (8, 20, 21, 69), the AKLT spin-1 chain (15), transverse field Ising ladders (70), a domain wall conserving spin-1/2 model (18), models with multiple magnons (19, 27), and various chiral

and nonchiral fermionic models (24, 71, 72) can be understood using at least one of the three descriptions. As the SGA is most closely connected to the quasiparticle perspective, we describe it below

A quasiparticle creation operator Q^+ provides an SGA if its commutator with the Hamiltonian H_{SG} satisfies

$$[H_{SG}, Q^+] = \omega Q^+$$
 18.

for $\omega \neq 0$. If $|\psi_0\rangle$ is an eigenstate of H_{SG} with eigenvalue E_0 , then $(Q^+)^n |\psi_0\rangle$ is also an eigenstate with eigenvalue $E_0 + n\omega$ for any integer n > 0 (as long as $(Q^+)^n |\psi_0\rangle \neq 0$). The SGA thus provides multiple towers of equally spaced eigenstates.

Often, however, Equation 18 asks for too much and results in special towers of states for symmetry reasons. For example, consider the SU(2) algebra defined in Equation 8 that arises in the description of the scar tower in the spin-1 XY model. Suppose that we define a Hamiltonian of the form $H_{SG} = H_{\text{sym}} + \omega J^z$, where H_{sym} is J-SU(2) symmetric; i.e., it commutes with all of the generators in Equation 8. (An example of such an H_{sym} was found in Reference 19; see Equation 22 below.) The J-SU(2) raising operator J^+ then defines an SGA as in Equation 18, with $Q^+ = J^+$. In this scenario, the tower $|S_n\rangle$ in Equation 3 is not quantum many-body scarred, as each $|S_n\rangle$ has maximal J^2 eigenvalue and is the only state in its symmetry sector. It is precisely because the Hamiltonian of the spin-1 XY Hamiltonian H_{XY} in Equation 1 is not J-SU(2) symmetric that the tower of states $|S_n\rangle$ qualify as bona fide many-body scar states.

It is therefore useful to define the notion of a restricted SGA, which requires only that Equation 18 hold within the scarred subspace. That is, for a given vacuum state $|\psi_0\rangle$, if

$$H |\psi_0\rangle = E_0 |\psi_0\rangle,$$

$$[H, Q^+] |\psi_n\rangle = \omega Q^+ |\psi_n\rangle \,\,\forall \,\, n \text{ s.t. } (Q^+)^n |\psi_0\rangle \neq 0,$$

$$19.$$

then the states with n quasiparticles atop the vacuum state, $|\psi_n\rangle = (Q^+)^n |\psi_0\rangle$, are exact eigenstates of a Hamiltonian H with energies $E_0 + n\omega$. In practice, additional terms are added to SGA Hamiltonians to deform them into Hamiltonians that only satisfy Equation 19. Equation 1 represents one such deformation for the spin-1 case.

It is often the case that the stationarity of a few quasiparticle states, $|\psi_m\rangle$ for $m \leq M$, guarantees the stationarity of states with any number of quasiparticles atop the vacuum state, $|\psi_n\rangle$. For example, in the spin-1 XY chain, M=1, whereas in the AKLT chain M=2 (15). A rewriting of the condition in Equation 19 in terms of nested commutators then becomes useful (21):

$$H |\psi_0\rangle = E_0 |\psi_0\rangle, \qquad 20a.$$

$$\operatorname{ad}_{O^{+}}(H) |\psi_{0}\rangle = -\omega Q^{+} |\psi_{0}\rangle, \qquad 20b.$$

$$\operatorname{ad}_{Q^{+}}^{m}(H)|\psi_{0}\rangle = 0, \ 2 \le m \le M,$$
 20c.

$$ad_{O^+}^m(H) = 0, \ \forall \ m > M.$$
 20d.

Above, $ad_X(Y) = [X, Y]$. Solving the operator equation for m > M is much simpler than solving the restricted equation for $2 \le m \le M$ and provides valuable clues about the scarred states and/or the Hamiltonian H. For example, Reference 27 constructed operator bases that satisfied Equation 20d for a given Q^+ and M, whereas Reference 15 identified bimagnons as candidate stable quasiparticles for AKLT spin-1 chains by solving Equation 20d for M = 2.

¹Equation 18 has also been referred to in the literature as a dynamical symmetry (73–75).

2.3. Constructive Principles

There are several constructive principles that provide restricted SGAs and, thus, scarred Hamiltonians with certain species of stable quasiparticles. We focus here on a principle that leverages nonabelian symmetries and also discuss another mechanism based on particle confinement.

Nonabelian symmetries G furnish raising and lowering operators Q^{\pm} that naturally satisfy an SGA with (Cartan) generators Q^z in any subspace. When coupled with G-symmetric Hamiltonians and symmetric base states, we can construct large families of Hamiltonians with quasiparticle scar states (23):

$$H = H_{\text{sym}} + H_{\text{SG}} + H_A.$$
 21.

We now describe each of these terms.

The first term $H_{\rm sym}$ is G symmetric; that is, $[H_{\rm sym}, Q^\pm] = 0$ and $[H_{\rm sym}, Q^z] = 0$. (Note that, in general, $H_{\rm sym} = 0$ is also allowed.) Suppose the base state is an eigenstate of $H_{\rm sym}$. Then, $|\psi_0\rangle$ is labeled by its eigenvalue under the Casimir operator Q^z and the Cartan generator Q^z . Furthermore, $|\psi_n\rangle$ is a degenerate eigenstate with the same value of Q^z but a different value of Q^z . To guarantee that the base state is an eigenstate of $H_{\rm sym}$, it is often chosen to be an element of a unique irreducible representation (irrep) of the group G. For example, in the spin-1 XY model, the scarred states span the unique maximum-spin representation of the SU(2) algebra in Equation 8, to which the polarized state $|\Omega\rangle$ belongs. The J-SU(2) symmetric part of the spin-1 XY exchange Hamiltonian $H_{\rm XY}$ was found in Reference 20 to be given by

$$H_{\text{sym}} = \sum_{r} (|+_{r} 0_{r+1}\rangle \langle 0_{r} + |-_{r} 0_{r+1}\rangle \langle 0_{r} - |+_{r+1}| + \text{H.c.}).$$
 22.

The second term, H_{SG} , is a (linear combination of) generator(s) in the Cartan subalgebra of G so that $[H_{SG}, Q^{\pm}] = \pm \omega Q^{\pm}$. This term lifts the degenerate multiplets of H_{sym} into energetically equidistant towers of states. In the spin-1 XY model, $H_{SG} = bS^z = 2bJ^z$ so that $\omega = 2b$.

The final term in Equation 21 breaks the *G* symmetry but annihilates the scar states: $H_A |\psi_n\rangle = 0$. In the spin-1 XY model of Equation 1, it is given by $H_A = J(H_{XY} - H_{sym})$, where H_{sym} is given in Equation 22. Explicitly (19),

$$H_{A} = J \sum_{r} \left[\left(\left| +_{r} -_{r+1} \right\rangle + \left| -_{r} +_{r+1} \right\rangle \right) \left\langle 0_{r} 0_{r+1} \right| \ + \ 2 \left| -_{r} 0_{r+1} \right\rangle \left\langle 0_{r} -_{r+1} \right| \ + \ \text{H.c.} \right].$$

The symmetry-based formalism is powerful because of its generality. First, G can be any continuous nonabelian symmetry group or a q-deformed version thereof (23, 26). Indeed, there are examples of scarred models in the literature in which G is SU(3) (23), q-deformed SU(2) (23), or U(N) or SO(N), where N is the number of lattice sites (24), etc. Second, even when G is SU(2), it need not be the spin-SU(2). Prominent examples include the Hirsch model with η -pairing states as scarred states (20) and generalized AKLT models (76). Third, the scar tower need not be an irrep of G with maximal eigenvalue under the Casimir operators. In the SU(2) case, for example, the base state could be a single-magnon state with zero quasimomentum and S = L/2 - 1 (27). Indeed, the scar tower need not be an irrep of G at all if H_{sym} is special and multiple irreps are degenerate. The scarred bimagnon tower in the AKLT model provides such an example (19). Fourth, the same symmetry group G can provide multiple raising operators J^+ to embed scar pyramids (19, 27). For example, with G = SU(2), single-magnon excitations with multiple momenta (k = 0 and $k = k_0$ for any k_0) can be infinitely long-lived excitations atop the fully polarized state.

There are a few examples of scarred models that do not obviously fit into the symmetry-based formalism. For instance, in the domain-wall conserving model of Reference 18 the quasiparticle creation operator Q^+ does not a have a clear connection to a root of a Lie algebra. Another

example, surprisingly, arises in the spin-1 XY model, which hosts a second tower of so-called bond-bimagnon states (17, 22). The quasiparticle creation operator for this tower of states is so far not known. However, in both of these examples, the towers of states arise from the projection of an auxiliary tower of states that transform as a representation of a Lie algebra (18, 22, 68).

An interesting application of the symmetry-based formalism is to deformations of integrable points. Integrable points have extensively many continuous symmetries and, thus, provide extensively many creation operators Q^+ of distinct quasiparticles. A suitable deformation H_A could preserve one or several of these quasiparticles as infinitely long-lived excitations. The deformation of integrable points thus provides a systematic way to construct large families of quantum scarred models. An early study of a deformed PXP model suggested that this model is proximate to integrability (77), which might explain the origin of scarring in it (see Section 4 for further discussion). Integrability also played an important role in scars that were experimentally obtained in a 1D dysprosium quantum gas (78). Theoretically, the connection between scars and integrability has been studied in References 23, 71, 76, and 79–81, but this is still largely unexplored territory.

How to construct the all-important H_A that breaks the global symmetry? There are several methods discussed in the literature.

One method is to use local projectors that annihilate local patterns that appear in the scarred tower. Such projectors can be constructed using the symmetry *G* itself. For example, References 26 and 68 construct the subspace generated by the action of *G* on the base state restricted to a small number of sites; the complement of this subspace provides the required local projector. The result is a frustration-free Hamiltonian, discussed further in Section 3.1.

Another method is to choose the group G so that the scarred subspace is a singlet of the group (24, 25). In this case, any $H_A = \sum_a O_a T_a$, where T_a are the generators and O_a are any operators that make H_A Hermitian, annihilating the scarred subspace. Note that, in this case, H_{sym} need not be G-symmetric—it need only have the G singlets as eigenstates (see 24 and 25 for more details).

Brute force computation in an operator basis is also useful. That is, we search for coefficients c_a of a set of translationally invariant operators $O^a = \sum_i O_i^a$ such that $H_A = \sum_a c_a O^a$ annihilates all the states in the scarred manifold. When the SGA is furnished by a symmetry, choosing the operators O^a to be irreducible tensor representations sets several c_a to zero on symmetry grounds (27). The remaining c_a satisfy simple linear relations, which can be solved analytically or numerically (23, 27, 82). The resulting H_A generically does not annihilate the scarred states term by term. Such Hamiltonians are thus referred to as as-a-sum annihilators.

Other methods use the language of matrix product states and operators to construct nearest-neighbor Hamiltonians with a quasiparticle tower of scars (68, 76). The starting point is to write the states with n quasiparticles, $|\psi_n\rangle = (Q^+)^n |\psi_0\rangle$, as matrix product states using two types of matrices for each site depending on whether there is or is not a quasiparticle on that site. Enforcing that the quasiparticles cannot sit on neighboring sites results in simple algebraic conditions on parent Hamiltonians with the scarred tower $|\psi_n\rangle$. This method was used to discover several AKLT-type models with bimagnon scars atop a spin liquid ground state (19, 76), perturbed Potts models with trimagnon scars (76), and a two-dimensional model with topologically ordered states within the scarred subspace (68).

As an aside, we note that none of the constructions described above guarantee that H_A exclusively annihilates the scarred subspace. Indeed, determining the number of states annihilated by a local Hamiltonian is in general intractable, although interesting lower bounds exist (83).

References 84 and 85 suggest that particle confinement leads to quantum many-body scars at varying energy densities. Specifically, References 84 and 85 study the ordered phase of the Ising model in transverse and longitudinal fields in one dimension. The longitudinal field leads to

confinement of domain walls, so that a pair of domain walls forms a bound state (a meson) whose energy grows with their separation. These single meson states persist as eigenstates well above the two-meson threshold; they apparently persist even when the two domain walls are macroscopically separated and the state has a finite energy density above the ground state. Whether the persistence is only a finite-size effect in the lattice model and whether other continuum models that are in confined phases exhibit scars are open questions.

3. GENERALIZED SCARS BEYOND QUASIPARTICLES

In this section, we broaden our scope beyond quasiparticles and return to the connection of scars with the failure of thermalization mentioned in the Introduction. The purpose of this section is, in part, to chart out the historical genesis of scars and also to provide an overview of the richness of phenomena that have been associated with the term scar, but which at times refer to some rather distinct types of underlying physics.

3.1. Scars from Projector Embeddings

Perhaps the earliest mention of the existence of a special eigenstate of a Hamiltonian that passes robustly, with perfectly unavoided crossings, through other states as parameters of the Hamiltonian are varied was provided by Shastry & Sutherland (86). In their eponymous spin model, an exactly dimerized state remains an eigenstate even when it ceases to be the ground state of the model. This kind of scar state does not come with a tower of states at all—it is a priori just an individual very special state that happens to escape eigenstate thermalization.

The Shastry–Sutherland model is an example of an important class of Hamiltonians known as frustration-free Hamiltonians. Such Hamiltonians can be written (up to a constant energy shift) as a sum of local projection operators P_i ,

$$H_{\rm FF} = \sum_{i} b_i P_i,$$
 24.

with real coefficients $b_i \ge 0$. The ground state or states of frustration-free Hamiltonians are states $|\psi_{FF}\rangle$ that satisfy $P_i |\psi_{FF}\rangle = 0$ for all i. Note that two projectors P_i and P_j in the Hamiltonian Equation 24 need not commute with each other, so that H_{FF} may be nonintegrable. In addition to the Shastry–Sutherland model, well-known examples include the AKLT and Klein models (60, 87), the Rokhsar–Kivelson model (88) and its generalizations (89), the toric code (90), and other parent (91–93) and uncle (94) Hamiltonians for matrix product states.

It is always possible to modify a frustration-free Hamiltonian such that a ground state of the original model becomes an arbitrarily highly excited state of the modified model. For example, in Equation 24, one can modify the coefficients b_i to have both positive and negative signs, in addition to varying magnitudes, or even promoting b_i to arbitrary local operators. The erstwhile ground states $|\psi_{FF}\rangle$ then remain zero-energy states of the modified Hamiltonian.

The connection of these ideas to the ETH was first drawn by Shiraishi and Mori (SM) in References 95 and 96. The SM construction again relies on the existence of an extensive set of local projectors $\{P_i\}$, and a target scarred subspace \mathcal{T} spanned by states annihilated by the local projectors: $P_i|\psi\rangle = 0 \ \forall i$. The SM Hamiltonian is a sum of two terms: The first is a (modified) frustration-free Hamiltonian H_A that annihilates any state in the target subspace \mathcal{T} , and the second term H' commutes with all the projectors P_i ($[H', P_i] = 0$):

$$H_{\rm SM} = \underbrace{\sum_{i} P_i b_i P_i + H'}_{H_A}, \qquad 25.$$

where b_i are arbitrary local Hamiltonians. The Hamiltonian is constructed to be block-diagonal because H' does not mix states in \mathcal{T} with those in its complement $\overline{\mathcal{T}}$. Thus, $H_{\rm SM}$ can be diagonalized in \mathcal{T} and $\overline{\mathcal{T}}$ independently. The energy eigenvalues of the eigenstates $\{|\psi\rangle_t\}$ in \mathcal{T} are set entirely by H'. These could be interleaved anywhere within the spectrum of $H_{\rm SM}$, including at an energy density corresponding to infinite temperature. However, the other states at the same energy density in $\overline{\mathcal{T}}$ are expected to reproduce thermal expectation values, as H_A (and thus $H_{\rm SM}$) should be nonintegrable for generic Hermitian b_i . For example, the expectation value of the local projector P_i in any of these states should be proportional to $\operatorname{tr}(P_i)$. The same expectation value in a scarred eigenstate is exactly zero, at odds with the ETH.

It is useful to briefly discuss the embedded states in relation to possible symmetries of H_{SM} . The ETH holds only within individual symmetry sectors. SM presented their embedded states as counterexamples to the ETH because H_{SM} generically does not have any obvious local symmetries, and so the embedded target states need not live in a separate symmetry sector from the rest of the spectrum. Crucially, the P_i 's do not generically form a mutually commuting set and, hence, are not a set of local symmetries for the Hamiltonian.²

An alternative perspective is to think of \mathcal{T} and $\overline{\mathcal{T}}$ as disconnected subspaces that do not couple to each other under the action of H_{SM} . In other words, H_{SM} can be decomposed as

$$H_{\text{SM}} = H_{\mathcal{T}}^{\text{scar}} \oplus H_{\overline{\mathcal{T}}}^{\text{thermal}}.$$
 26.

Several examples of embedded towers of states with quasiparticles lie within the SM construction. Remarkably, the spin-1 XY bimagnon scar tower also falls into this class, although the model was not explicitly constructed using the SM formalism. The projection operators associated with the embedding are given by

$$P_r = 1 - \frac{3}{4} (S_r^z)^2 (S_{r+1}^z)^2 + \frac{1}{8} \left[(S_r^+)^2 (S_{r+1}^-)^2 + \text{H.c.} \right] - \frac{1}{4} S_r^z S_{r+1}^z.$$
 27.

We refer the reader to Reference 17, appendix C, for a more detailed discussion. The SM method has also been used to embed a macroscopic SU(2) spin (66), multiple towers of magnon states (27) and magnon crystals (98, 99), as well as states with no quasiparticle interpretation, e.g., zero modes in gauge theories (100, 101), topologically ordered states (102–104), and states in geometrically frustrated systems (98, 105).

3.2. Hilbert Space Fragmentation

We now turn to a related but conceptually distinct mechanism for ergodicity breaking, which does not rely on eigenstates or even time periodicity of the dynamics. This phenomenon is variously described as "Hilbert space shattering" (106), "Hilbert space fragmentation" (107), or "Krylov fracture" (108) and refers to the existence of an exponentially large number of dynamically disconnected sectors of Hilbert space. This fragmentation of Hilbert space can be viewed as a generalization of the emergence of dynamically disconnected subspaces discussed in the previous section.

The most familiar way to obtain dynamically disconnected sectors is through the existence of conservation laws, with different sectors labeled by the values of conserved quantities. Thermodynamically, it is the sector with the lowest free energy that determines the physical behavior, but if a system is initialized in a different symmetry sector, observables are determined by the statistical properties of that sector.

²However, when the projectors do commute, the disconnected sectors can be interpreted as being distinguished by symmetry (97).

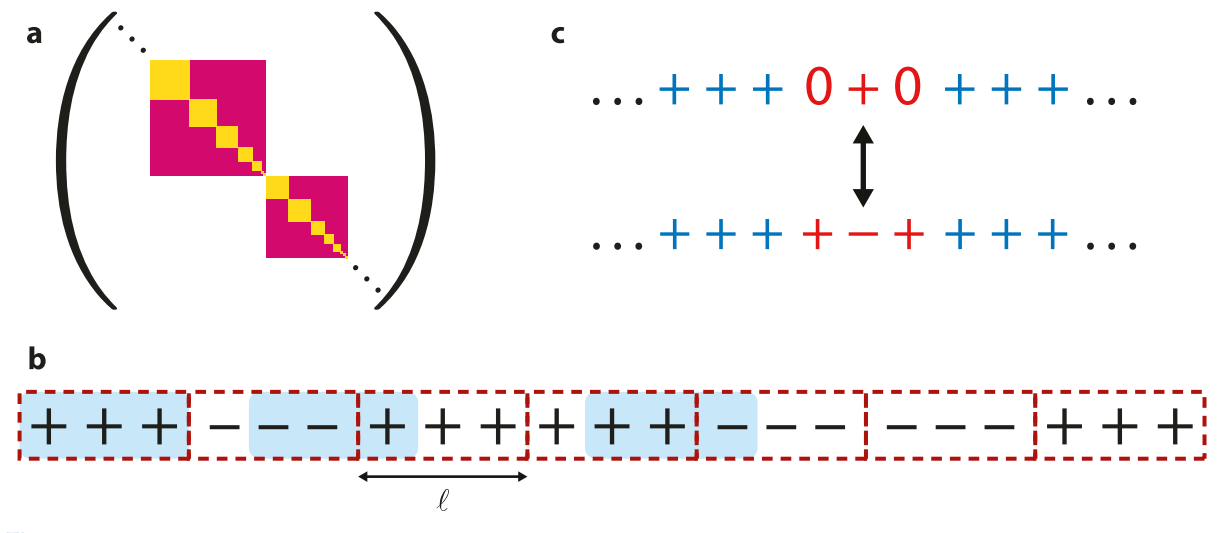


Figure 2

A mechanism for Hilbert space fragmentation. (a) Schematic of the block structure of the evolution operator in a system with Hilbert-space fragmentation. The pink blocks denote different symmetry sectors, whereas the yellow blocks denote disconnected Krylov subspaces. (b) Example of a frozen state in a one-dimensional spin-1 chain with U(1) charge and dipole-moment conservation acted upon by local gates with range at most $\ell=3$. Any gate acting on three consecutive sites (e.g., the shaded blue regions) cannot change the state because the local configuration has either extremal charge (as in the leftmost block) or dipole moment (as in the middle and rightmost blocks). (c) Example of a two-dimensional Krylov subspace generated by an active region (red) embedded in a frozen background (blue). The transition indicated by the black arrow is the only one allowed by charge and dipole conservation. Panel b adapted from Reference 106.

By contrast, interesting examples of Hilbert space fragmentation involve the existence of dynamically disconnected sectors even after resolving all microscopic symmetries—i.e., states with the same symmetry quantum numbers are still forbidden from mixing under the dynamics (106, 107; see **Figure 2a**). The unitary operator governing the time-evolution thus has a block diagonal structure (in some simple basis), which reflects both the symmetries of the problem and further fragmentation within symmetry sectors. Strikingly, for systems with one or a few symmetries, while the number of symmetry sectors generally scales at most polynomially with system size, the number of dynamical sectors can scale exponentially with system size. The dimension of the individual sectors can range from one (corresponding to a single frozen state) to exponential in system size. A further distinction between strong and weak fragmentation can be made depending on whether the ratio of the dimension of the largest dynamical sector to that of its symmetry sector tends to zero or one in the thermodynamic limit, respectively (106, 107). In the former (strong) case, there is an exponential number of dynamically disconnected sectors, which can lead to nonthermalizing dynamics even from typical initial states. The latter (weak) case is more generic and predicts thermalization to the appropriate thermodynamic ensemble from most initial states.

Fragmented dynamics is considered scarred because of (a) a strong initial state dependence in the dynamics, ranging from fully localized to typically thermal depending on the dynamical sector in which one starts, and (b) anomalous or frozen dynamics from simple low-entanglement initial states never thermalize to the equilibrium state appropriate to the symmetry quantum numbers of the initial state.

The dynamical sectors are also referred to as Krylov sectors, following standard prescriptions for constructing the Krylov subspace \mathcal{K} of a state $|\psi_0\rangle$ time-evolving under a Hamiltonian H: The state $e^{iHt}|\psi_0\rangle$ lives in the span of all vectors obtained by the repeated action of H on $|\psi_0\rangle$,

 $\mathcal{K} = \operatorname{span}\{|\psi_0\rangle, H|\psi_0\rangle, H^2|\psi_0\rangle, \cdots\}$. In the cases of most interest, the states $|\psi_0\rangle$ are simple experimentally preparable states (such as product states), and the dimension of \mathcal{K} is a vanishing fraction of the full Hilbert space dimension, leading to Krylov restricted thermalization within \mathcal{K} (108); in certain cases, the dynamics in \mathcal{K} may be integrable even if the model as a whole is not (108, 109). Recent works have constructed integrals of motion that label disjoint Krylov subspaces. In systems with Hilbert space fragmentation, there are exponentially many such integrals of motion that need not be sums of local operators (110, 111).

A transparent manifestation of Hilbert space fragmentation occurs in local systems that conserve both a global U(1) charge and its dipole moment (106, 107, 112). In a one-dimensional spin system, these symmetries take the form $Q = \sum_x S_x^z$ and $P = \sum_x x S_x^z$, where the sum is over all lattice sites. These symmetries are characteristic of fracton topological phases (for reviews of fractons, see 113 and 114), and their combination produces $O(L^3)$ symmetry sectors labeled by (Q and P) quantum numbers in a system of size L. In contrast, these symmetries are provably sufficient to produce exponentially many dynamical subsectors, including exponentially many strictly frozen product states that live in dynamical subspaces of dimension exactly equal to one. In addition to the frozen states, there is a wide distribution of dimensions for the emergent subsectors, leading to a strong initial state dependence in the dynamics. The fragmentation is robust to the presence of both spatial and temporal randomness as long as the symmetries and locality are maintained.

The existence of exponentially many strictly frozen states is readily verified by the following simple argument (106). It is easiest to think of random unitary circuit models in which each unitary gate has range ℓ and each gate locally conserves Q and P. Let us denote by +/- the maximum/minimum local charges on a site, respectively; these could be the top and bottom states of a qudit of spin S so that $S^{\circ}=\pm S$. Now, note that any pattern that alternates between locally all plus and locally all minus, with domain walls between all-plus and all-minus regions at least ℓ sites apart, must be inert by local charge and dipole moment conservation. **Figure 2**b shows an example of such a frozen configuration with S=1 and $\ell=3$. A straightforward lower bound on the number of such frozen states can be obtained by dividing up the L-site chain into blocks of size ℓ . Because all spins in each block must be either + or -, there must be at least $2^{L/\ell}$ such frozen states. This is exponentially large in L for any finite ℓ , but such frozen states still constitute a vanishing fraction of the full Hilbert space. For a more precise counting, see, e.g., Reference 106.

Other sectors with dimension larger than one can be systematically built by embedding dynamically active blocks into sufficiently large frozen backgrounds so as to keep the active region localized to a finite region of space; see **Figure 2***c* for a simple example.

It is also easy to write down Hamiltonians with charge and dipole conservation, for instance, Hamiltonians with coordinated pair hopping terms $|1001\rangle \leftrightarrow |0110\rangle$. Such Hamiltonians arise when considering models of the fractional quantum Hall effect in thin cylinders, i.e., in a quasi-1D limit (108, 115–117). Such pair hopping terms could also emerge as the leading-order description of systems placed in large electric fields (106, 108). Dipole moment couples directly to electric field, so if the system is placed in a sufficiently large static electric field (or equivalently, a tilted potential), then the Hilbert space will (approximately) split into symmetry sectors labeled by dipole moment (equivalently, center of mass position), with states at different dipole moment having sharply different energies. Equivalently, such systems can be viewed as possessing an emergent prethermal conservation of dipole moment that disappears after an exponentially long timescale (106, 118, 119). Much recent theoretical and experimental (120–122) work has focused on such tilted systems, with claims that there may be a phase transition to a so-called Stark MBL (123, 124) phase in which a disorder-free system becomes many-body localized above a

critical value of the tilt strength. However, it has been argued that the numerical signatures of Stark MBL may instead be finite-size and -time effects due to apparent Hilbert space fragmentation from long-lived prethermal dipole conservation induced by the tilted potential (106). One can also consider conservation of higher multipole moments in higher dimensions, which have been shown to be associated with slow subdiffusive hydrodynamics (125–127).

Analogous physics has been studied in various other contexts including, e.g., interacting fermion models (108, 128-130), models with kinetic constraints (including in classical settings; 109, 131–136) and multicomponent Hilbert spaces (75, 137), and models with emergent gauge fields such as frustrated magnets and dimer models (98, 138, 139). The existence of dynamically disconnected sectors and the resulting danger of obtaining thermodynamically incorrect results by getting trapped in an atypical sector have also been appreciated for a long time by the numerical simulation community (138, 140)—this is the flip side of using Hilbert space fragmentation to obtain nonthermal behavior. This goes along with autonomously interesting investigations of the sector structure of such models (see, e.g., 141). The possibility of obtaining disorder-free glassy dynamics has also been discussed in this context (see, e.g., 131, 142-147). However, we note although dynamics in these various other settings can be described by the existence of dynamically disconnected subsectors, there is no understanding of general (i.e., constructive) conditions that lead to Hilbert space fracture in these models and no principled way to examine the stability of fracturing in these models to the addition of perturbations or noise. For example, the simplest kinetically constrained models comprise spin-1/2 systems in which the spin on a site can flip if certain conditions are obeyed by its neighbors, for instance, if both neighbors are down. However, there is no unique or natural way to deform such models, for example, to include the effect of further neighbor spins. Likewise, the dynamics in quantum dimer models come from certain flippable plaquettes that are lattice dependent. Although allowing for longer flippable loops decreases fracture (138, 140), there are no general results on how the number of disconnected sectors scales with such perturbations. In contrast, the dipole-conserving models discussed here provide a robust symmetry-based constructive mechanism for Hilbert space fracture.

4. EXPERIMENTS AND THE PUZZLES THEY INSPIRE

Much of the present interest in quantum many-body scars originates from an experiment reported in Reference 59, which observed unexpected coherent oscillations in a system of interacting Rydberg atoms when the array was prepared in a particular initial state. (Further systematic experimental analysis of this phenomenon was undertaken in Reference 148.) In this section, we summarize this experiment and the theoretical attempts to understand it, making connections and drawing contrasts with the quasiparticle-centric point of view adopted in this review. We close this section with a summary of other experiments that have been performed in this domain. Throughout, we emphasize the remaining theoretical puzzles.

4.1. Rydberg Atom Experiment and the PXP Model

In Reference 59, a system of rubidium atoms trapped in optical tweezers was used to perform an analog quantum simulation of the one-dimensional Ising model in transverse and longitudinal fields. The array of atoms is driven in such a way that each atom can be in either its ground state or a highly excited Rydberg state. The resulting system can be viewed as an array of coupled two-level systems, described by Pauli operators Z_i and X_i , with Hamiltonian

$$H = \sum_{i < j} V_{ij} n_i n_j - \Delta \sum_i n_i + \frac{\Omega}{2} \sum_i X_i.$$
 28.

Here, $n_i = (1 + Z_i)/2$ is the occupation of the Rydberg state of the *i*th atom, and X_i couples the *i*th atom's ground and Rydberg states. The parameter Ω is the Rabi frequency of the driving laser, and Δ is the detuning of the driving laser from the Rydberg state. The coupling $V_{ij} > 0$ originates from van der Waals interactions between excited atoms and falls off as R_{ij}^{-6} with the distance R_{ij} between atoms *i* and *j*. When the nearest-neighbor interaction strength $V \equiv V_{i,i+1}$ is much stronger than both $V_{i,i+2}$ and Ω , the system enters the so-called Rydberg-blockade regime in which nearest-neighbor atoms cannot simultaneously be excited (149). The leading-order effective Hamiltonian in this regime can be written as

$$H_{\text{eff}} = \sum_{i} \left(\frac{\Omega}{2} P_{i-1} X_i P_{i+1} - \Delta n_i \right),$$
 29.

where the projector $P_i = (1 - Z_i)/2$ ensures that the Rydberg-blockade constraint is satisfied and where longer-range interaction terms V_{ij} with |i-j| > 1 have been neglected. This effective model has a history dating at least as far back as Reference 150, and, when $\Delta = 0$, is known as the PXP model. The model is also relevant to U(1) lattice gauge theory in its quantum link (151) and dimer model (152–154) formulations and to the fractional quantum Hall effect at $\nu = 1/3$ in the thin-torus limit (117).

As an aside, the form of the model in Equation 29 reflects one of the central themes in the physics of (especially topological) correlated quantum matter. Demanding that the largest term in a Hamiltonian be satisfied requires the identification of, and projection onto, the resulting physical subspace. This is the case here with the Rydberg blockade, and appears analogously in the avoidance of double occupancy in high-temperature superconductors via a Gutzwiller projection (155, 156), in enforcing the ice rules in spin ice, yielding an emergent magnetostatics (157), or in minimizing kinetic energy in quantum Hall physics by projecting onto a partially filled Landau level (158).

The experiment in Reference 59 prepared a Néel initial state, which can be expressed in the Rydberg occupation basis as $|\mathbb{Z}_2\rangle = |101\ldots\rangle$, and evolved it with the Hamiltonian in Equation 28 with $\Delta=0$ in the Rydberg blockade regime. When $\Delta=0$, the average energy $\langle\mathbb{Z}_2|H_{\rm eff}|\mathbb{Z}_2\rangle$ lies in the middle of the spectrum of the nonintegrable model $H_{\rm eff}$ —i.e., $|\mathbb{Z}_2\rangle$ is effectively an infinite-temperature state in the Rydberg-blockaded subspace. Thus, the expectation based on the ETH is that the dynamics of this initial state should rapidly decohere, and local observables should thermalize to their infinite temperature expectation value; nevertheless, coherent oscillations of the occupation numbers n_i were observed about a nonthermal value. Concurrent theoretical work reported in Reference 59 found that the entanglement entropy following this quench from the Néel state grows much more slowly than for other product states and also exhibits oscillations at the same frequency.

Expanding the Néel state in the eigenbasis of Equation 29 shows that the unexpected oscillations can be traced back to a set of (L+1) special low-entanglement eigenstates in the spectrum of the PXP model for a chain of L sites. This set of eigenstates spans the entire many-body bandwidth of the PXP model in the sector with no nearest-neighbor Rydberg excitations and includes both the ground state and the highest-energy state. These eigenstates, which were termed quantum many-body scar states in Reference 12, have anomalously high overlap with the $|\mathbb{Z}_2\rangle$ state and are approximately equally spaced in energy, leading to coherent oscillatory dynamics of a variety of quantities and periodic near-revivals in the Loschmidt echo $\mathcal{L}(t)$ (see Equation 14). Follow-up work in Reference 159 found that the scar states also have anomalously low entanglement relative to other eigenstates of the PXP model at the same energy density, with half-chain entanglement entropy scaling $\sim \ln L$.

4.2. Attempts to Understand Scars in the PXP Model

Although the existence of low-entanglement scarred eigenstates in the PXP model provides a descriptive explanation of the experimental observations of Reference 59, a complete understanding of why this model contains scars is still lacking. We now describe various attempts to understand the origin of the scarred eigenstates in the PXP model.

One line of work originated by the authors of References 12 and 159, known as the forward scattering approximation (FSA), constructs the scar states using a Krylov subspace approach. In this approach, the PXP Hamiltonian, $H_{PXP} = \sum_{i} P_{i-1} X_i P_{i+1}$, is broken up as

$$H_{\text{PXP}} = H^+ + H^-,$$
 30a.

where

$$H^{+} = \sum_{i \text{ odd}} P_{i-1} \sigma_{i}^{-} P_{i+1} + \sum_{i \text{ even}} P_{i-1} \sigma_{i}^{+} P_{i+1},$$
 30b.

and $H^+ = (H^-)^{\dagger}$. The operators H^{\pm} act as raising and lowering operators for the staggered magnetization $Z_{\pi} = \frac{1}{2} \sum_{i} (-1)^{i} Z_{i}$; i.e.,

$$[Z_{\pi}, H^{\pm}] = \pm H^{\pm}.$$
 31.

The Néel state $|\mathbb{Z}_2\rangle$ is the minimum-eigenvalue eigenstate of Z_π . For a chain of L sites, one can therefore define a Krylov subspace $\mathcal{K} = \{|0\rangle, |1\rangle, \ldots, |L\rangle\}$ spanned by L+1 states $|k\rangle \propto (H^+)^k |\mathbb{Z}_2\rangle$, so that $|0\rangle = |\mathbb{Z}_2\rangle$ and $|L\rangle = |\mathbb{Z}_2'\rangle = |010\ldots\rangle$. Approximations to the scar states are then obtained by diagonalizing the projection of H_{PXP} into the subspace \mathcal{K} , which is a matrix of dimension L+1. The FSA thus allows one to obtain approximations to the scarred eigenstates of the PXP model at system sizes much larger than those accessible to exact diagonalization and, as shown in Reference 159, produces eigenstates with entanglement entropy scaling as $\ln L$. More recently, Reference 160 found a nonlocal interacting model for which the FSA becomes exact. However, this model is not perturbatively connected to the PXP model.

Equation 31 is suggestive of an SU(2) algebra generated by H^{\pm} and Z_{π} and, thus, of an SGA. However, as noted in Reference 66, this algebra is not closed, because

$$[H^+, H^-] = \frac{1}{2} Z_{\pi} + \frac{1}{4} O_{ZZZ},$$
32.

where we have assumed periodic boundary conditions and defined $O_{ZZZ} = \sum_{i} (-1)^{i} Z_{i-1} Z_{i} Z_{i+1}$. We revisit the SGA connection below.

Subsequent work in Reference 161 unified the FSA approach with parallel works that described the oscillatory scarred dynamics in the PXP model using the time-dependent variational principle (TDVP; 162–164). The TDVP is a semiclassical approach that projects the quantum dynamics of a system into a variational manifold of matrix product states (165), leading to a set of classical equations of motion that can exhibit phenomena familiar from the theory of classical chaos. In this way, the FSA can be brought into contact with the theory of quantum scars in single-particle quantum mechanical systems arising as quantizations of classical dynamical systems (13). However, though the TDVP approach captures the scarred dynamics in the space of variational matrix product states with low bond dimension (and hence low entanglement entropy), the periodic orbits may disappear on increasing the bond dimension (164). More work is thus required to sharpen the connection to single-particle scars.

A parallel strand of works have taken inspiration from the tower-like structure of the scar states, as evidenced by their nearly constant energy spacing and logarithmically scaling entanglement entropy, to attempt to formulate a quasiparticle description of these states.

One manner in which a quasiparticle description of the scar states can arise is through proximity to an integrable model, where every eigenstate can be described in terms of quasiparticles (166). The proximity to integrability further guarantees that the dynamical response of the integrable model survives for a parametrically long time (167–173). The connection between the PXP model and integrability was first pointed out in Reference 77, which found that adding

$$H_{XZ} = h_{XZ} \sum_{i} P_{i-1} X_{i} P_{i+1} (Z_{i-2} + Z_{i+2})$$
 33.

to $H_{\rm PXP}$ with a small coefficient $b_{\rm XZ} \simeq -0.02$ both strengthened the revivals and pushed the model closer toward integrability (as measured by various diagnostics such as Poisson statistics in energy-level spacings and fluctuations of eigenstate expectation values). Intriguingly, $H_{\rm XZ}$ and its longerrange generalizations also enhance the accuracy of the FSA (66)—albeit with a different value of $b_{\rm XZ}$ —and have a simple physical origin in complete bipartite graphs (174). However, whether there exists an exact integrable point in the vicinity of $H_{\rm PXP} + H_{\rm XZ}$ remains unknown.

Another possibility is that the PXP model is proximate to a nonintegrable model with a single infinitely long-lived quasiparticle species atop a vacuum state, similar to the case of the spin-1 XY model discussed in Section 2.1. (Of course, this tower may still be obtained by adding an appropriate H_A to a parent integrable/high-symmetry model as discussed in Section 2.3.) Reference 175 constructed an approximate tower of momentum– π magnon states atop the ground state of the PXP model and showed that the scar states found in Reference 12 have high overlap with this tower. The ground state, which we call $|E_0\rangle$, is known to be paramagnetic and has an efficient variational representation given in Reference 176. The lowest-lying excitation atop this ground state was shown numerically in Reference 175 to have high overlap with the state $S^+_{\pi}|E_0\rangle$, where

$$S_{\pi}^{\pm} = Z_{\pi} \mp i\alpha Y_{\pi}; \qquad 34.$$

here, Z_{π} is the staggered magnetization, $Y_{\pi} = \frac{1}{2} \sum_{i} (-1)^{i} P_{i-1} Y_{i} P_{i+1}$, and $\alpha \approx 2$ is a constant determined by numerical optimization. This excitation is naturally interpreted as a magnon with momentum π . Similar excitations can be created atop the highest excited state of the model, $|E_{\text{max}}\rangle$, via $S_{\pi}^{-} |E_{\text{max}}\rangle$. This observation motivates the definition of a variational subspace spanned by π magnon states,

$$V_{\pi} = \operatorname{span}\{(S_{\pi}^{+})^{n} | E_{0} \rangle, (S_{\pi}^{-})^{m} | E_{\max} \}_{n,m=0}^{L/2},$$
35.

in which the tower of scar states has substantial weight at finite system sizes. Furthermore, enlarging the variational basis with states in which magnons have nontrivial relative momenta, e.g., $(S_{\pi}^+)^{n-2}S_{\pi-\delta k}^+S_{\pi+\delta k}^+|E_0\rangle$, systematically increases the weight of the scar states in the variational magnon subspace.

Let us now revisit the connection to SGAs. Setting $\alpha = 2$ in Equation 34, one finds that (175)

$$[S_{\pi}^{+}, S_{\pi}^{-}] = 2 H_{\text{PXP}},$$

 $[H_{\text{PXP}}, S_{\pi}^{\pm}] = \pm S_{\pi}^{\pm} \pm O_{ZZZ},$

$$36.$$

where O_{ZZZ} is defined below Equation 32. Up to the extra O_{ZZZ} term in the second line, this is an SU(2) algebra. Equation 36 can be viewed as analogous to Equations 31 and 32, except that the roles of Z_{π} and H_{PXP} have been interchanged. This point of view suggests a conceptual link between the FSA and the quasiparticle picture of Reference 175.

One consequence of the algebra in Equation 36 is the prediction of off-diagonal long-range order in the scar states (see the discussion around Equation 10). Such eigenstate order would result in coherent oscillations of the two-time correlator $C_Y(t) = \langle \mathbb{Z}_2 | Y_{\pi}(t) Y_{\pi}(0) | \mathbb{Z}_2 \rangle / L^2$ in the thermodynamic limit (175, 177).

Alternative quasiparticle descriptions of the scar states in the PXP model have also been proposed. Reference 178 constructs a quasiparticle tower of states atop the ground state, similar to Reference 175, except it starts from a variational approximation to the ground state developed in Reference 179. In Reference 180, several exact matrix product state eigenstates of the PXP model were found near the middle of the energy spectrum, including at zero energy, where the model exhibits an exponentially large degeneracy (12, 181). Reference 180 constructed variational approximations to scar states near the middle of the spectrum by acting on the exact zero-energy matrix product eigenstates with local operators determined by numerical optimization. Note that this quasiparticle picture predicts that the scar states near the middle of the spectrum ultimately have area-law entanglement, because acting with a local operator on a finite-bond-dimension matrix product state can only increase the entanglement entropy by a finite amount in the thermodynamic limit. This would contradict the numerical finding of Reference 159 that the scar states have entanglement entropy $\sim \ln L$.

More recently, another quasiparticle picture was proposed in Reference 29. In that work, the PXP model is converted to an effective spin-1 chain using a mapping proposed in Reference 180. A tower of states is then constructed by acting on the fully polarized state of the effective spin-1 chain with an appropriate spin-1 lowering operator, followed by a projection operator that enforces the Rydberg-blockade constraint. This tower of states has the appealing property that the Néel state $|\mathbb{Z}_2\rangle$ can be written exactly as a superposition of the states in the tower, similar to the case of the spin-1 XY model in which the initial state $|\phi_0\rangle$ (Equation 13) can be written as a superposition of scar states. This work found numerically that the scar states of the PXP model have high overlap with this tower. Intriguingly, it also constructs a non-Hermitian extension of the PXP model for which the states in this tower are exact eigenstates.

One common theme that has arisen throughout the works described in this section is the hypothesis that the PXP model is proximate to a model with exact scars. The perturbation, Equation 33, proposed in Reference 77 and its longer-range variants considered in References 66 and 182 enhance revivals that are characteristic of scarred dynamics. These terms also enhance the accuracy of the FSA in Reference 12 and of the quasiparticle tower picture of Reference 175. Furthermore, Reference 29 found that terms of this form naturally emerge when trying to make their non-Hermitian model Hermitian. Reconciling these various perspectives where possible and determining the relationship (if any) to the model with an exact FSA proposed in Reference 160 remain interesting research directions.

4.3. Other Experiments

A variety of other experiments have detected signatures of many-body scarring. First, several recent experiments have realized the PXP model in other platforms. For example, Reference 183 used a Bose–Hubbard system in a tilted optical lattice to simulate the PXP model and measured entanglement and fidelity dynamics. Reference 177 used superconducting-qubit processors from IBM to realize the nearest-neighbor limit of the mixed-field Ising model, Equation 28, and probe the dynamics in the scarred regime, including measurements of the nontrivial correlator $C_Y(t)$. Another extension of the work performed in Reference 59 is that of Reference 148, which studied a periodically driven version of the PXP model and found intriguing subharmonic features in the dynamics of the Néel state.

Scars have also been realized in experimental platforms simulating other models. For example, in Reference 184 scarred dynamics were observed in a superconducting-qubit processor performing analog quantum simulation of a spin-1/2 XY model. In this work, the integrability of the spin-1/2 XY model is broken by random longer-range cross-coupling terms arising due to experimental imperfections, and scarred dynamics are observed from certain special initial states.

Reference 78 instead creates long-lived, highly excited but nonthermal states in a bosonic onedimensional quantum gas of dysprosium using a topological pumping mechanism. Starting from the ground state, the authors cyclically vary the contact interaction strength; as the Hamiltonian of the gas is close to an integrable one (the Lieb-Liniger model; 5, 185), this process maps one eigenstate to another higher up in energy instead of heating up the gas.

5. CONCLUSION AND OUTLOOK

In this review, we have considered the phenomenon of quantum many-body scarring through the lens of quasiparticles. We began by considering a relatively simple model of quantum many-body scars, the spin-1 XY model, where the existence of rare, nonthermal eigenstates can be shown analytically. The nonthermal eigenstates consist of a finite density of quasiparticles, known as bimagnons, with momentum π , whose scattering and dissociation are prevented by a destructive interference mechanism. We then moved on to consider more general settings for the realization of such towers of quasiparticle states, which can be formally understood in terms of SGAs and associated symmetry principles. We also reviewed a few constructive approaches to realize models with towers of many-body scar states. Subsequently, we considered a range of other contexts in which the nomenclature of scarring has been invoked, focusing in particular on projector Hamiltonians and the more extreme phenomenon of Hilbert-space fragmentation. Although these mechanisms for realizing nonthermal quantum many-body states have been associated with the phenomenon of scarring, they need not be associated with a quasiparticle description. Finally, we discussed experimental realizations of many-body scars, focusing in particular on the Rydberg experiment of Reference 59 and on the theoretical puzzles that it presents. Quasiparticles again appear in various guises in theoretical works attempting to explain these experimental results, but are not common to all theoretical descriptions that have been offered.

A variety of open questions remain. One of these concerns the stability of scarred many-body eigenstates to perturbations, which is crucially important both theoretically and in efforts to realize many-body scars in experiments. One way to phrase this question precisely is to ask, what is the timescale for an exact scarred eigenstate $|\psi_0\rangle$ of a nonintegrable Hamiltonian H_0 to thermalize under dynamics generated by $H_0 + \lambda V$, where V is some local perturbation and λ is a small parameter? Reference 186 presented an analysis of this problem on general grounds using Lieb–Robinson bounds and found that the thermalization time can be lower-bounded by $t_* \sim O(\lambda^{-1/(1+d)})$, where d is the spatial dimension of the system. This lower bound is extremely general and is likely not tight in many cases of interest. Whether tighter lower bounds can be obtained, and understanding the mechanisms by which the thermalization time can exceed this bound in specific cases, is an important question for future work.

Despite the large volume of theoretical work on the subject, another question that remains is the need to understand the origin of many-body scarring in the PXP model that is relevant to the original Rydberg experiment. Specifically, it would be desirable to understand whether there is a model, integrable or otherwise, in which the scarred eigenstates can be written down exactly. Even if such a model is found, however, there are other unusual features of the PXP model—for example, there are other spin-density-wave-like states, such as $|\mathbb{Z}_3\rangle = |100100...\rangle$, that exhibit approximate revivals (159), and other eigenstates that have anomalously high overlap with the Néel state $|\mathbb{Z}_2\rangle$ (187). Understanding these features of the model remains an outstanding challenge.

Although this review has focused on many-body scars in Hamiltonian systems, scars can also occur in other contexts. For example, many-body scars can appear in periodically driven systems, which do not conserve energy and are therefore expected to heat up to infinite temperature at late times (188, 189). There have been various studies of how such a heat death may be avoided, at least on long timescales (118, 119, 190). A variety of works, including the experiment in Reference 148,

have studied periodically driven variants of the PXP model (191–197) and found both exact and approximate scarring. Notably, for a particular choice of periodic driving, the PXP model can be fine-tuned to integrability (195–197). References 148 and 194 propose an intriguing connection between scarring and discrete time crystals (198–201) that deserves further exploration. Quantum scarring in the single-particle context can also occur in non-Hermitian systems (202), which motivates considering the possibility of many-body scars in this setting (73). Although there has been some initial progress in this direction (25, 29, 177), it would be interesting to consider more broadly the possibility of many-body scarring in open quantum systems. The notion of inverse scars, where thermal states are embedded in a nonthermal spectrum (203), may also be an interesting subject.

Finally, another important question concerns the range of systems in which many-body scars can be realized experimentally. So far, the vast majority of experimental efforts have focused on realizing the PXP model in different contexts. Only recently have experiments turned their attention to other models; for example, Reference 204 realized long-lived spin-helical states in a lithium atom system simulating anisotropic Heisenberg chains, and Reference 78 obtained scars in a dysprosium gas via topological pumping. However, whether scars stemming from other models and mechanisms could be observed in other experimental platforms is largely unexplored. The question of experimental realization is closely related to the exploration of potential applications for systems realizing quantum many-body scars. For example, References 205 and 206 show that systems with many-body scars can be useful in quantum sensing and metrology. Finding other potential applications of this fascinating phenomenon in quantum information science and technology is another worthy direction for future exploration.

DISCLOSURE STATEMENT

The authors are not aware of any affiliations, memberships, funding, or financial holdings that might reasonably be perceived as affecting the objectivity of this review.

ACKNOWLEDGMENTS

We are grateful to Nick O'Dea for preparing **Figure 1***b* and for previous collaboration, and to Andrei Bernevig and Maksym Serbyn for providing helpful feedback on the manuscript. We also thank our collaborators on previous works on scars and related topics in quantum dynamics, including Benjamin Burdick, Fiona Burnell, I-Chi Chen, Alexey Gorshkov, Christopher Langlett, Chris Laumann, Cheng-Ju Lin, Fangli Liu, Olexei Motrunich, Anne Nielsen, Peter Orth, Michael Schecter, N. Srivatsa, Long-Hin Tang, Julia Wildeboer, Shenglong Xu, Zhicheng Yang, and Yongxin Yao. We acknowledge valuable discussions with Jean-Yves Desaules, Wen Wei Ho, Timothy Hsieh, Ana Hudomal, Benjamin Lev, Sanjay Moudgalya, Zlatko Papić, Abhinay Prem, and Nicolas Regnault.

This work was supported in part by the National Science Foundation through awards DMR-1752759 (A.C.) and DMR-2143635 (T.I.), by the US Department of Energy, Office of Science, Basic Energy Sciences, under Early Career Award No. DE-SC0021111 (V.K.), and by the Deutsche Forschungsgemeinschaft under Cluster of Excellence ct.qmat EXC 2147 Project ID 390858490 (R.M.). V.K. also acknowledges support from the Sloan Foundation through a Sloan Research Fellowship and the Packard Foundation through a Packard Fellowship.

LITERATURE CITED

 Chaikin PM, Lubensky TC. 1995. Principles of Condensed Matter Physics. Cambridge, UK: Cambridge Univ. Press

- 2. Coleman P. 2015. Introduction to Many-Body Physics. Cambridge, UK: Cambridge Univ. Press
- 3. Moessner R, Moore JE. 2021. Topological Phases of Matter. Cambridge, UK: Cambridge Univ. Press
- 4. Bethe H. 1931. Z. Phys. 71(3-4):205-26
- Giamarchi T. 2003. Quantum Physics in One Dimension. Int. Ser. Monogr. Phys. Vol. 121. Oxford, UK: Clarendon
- Sutherland B. 2004. Beautiful Models: 70 Years of Exactly Solved Quantum Many-Body Problems. Singapore: World Sci.
- Essler FH, Frahm H, Göhmann F, Klümper A, Korepin VE. 2005. The One-Dimensional Hubbard Model. Cambridge, UK: Cambridge Univ. Press
- 8. Yang CN. 1989. Phys. Rev. Lett. 63(19):2144-47
- 9. Bhatt RN, McMillan WL. 1974. Phys. Rev. A 10(5):1591-97
- 10. Basko DM. 2017. Phys. Rev. Lett. 118:016805
- 11. Verresen R, Moessner R, Pollmann F. 2019. Nat. Phys. 15(8):750-53
- 12. Turner CJ, Michailidis AA, Abanin DA, Serbyn M, Papić Z. 2018. Nat. Phys. 14(7):745-49
- 13. Heller EJ. 1984. Phys. Rev. Lett. 53(16):1515-18
- 14. Venuti LC. 2015. arXiv:1509.04352
- 15. Moudgalya S, Rachel S, Bernevig BA, Regnault N. 2018. Phys. Rev. B 98(23):235155
- 16. Moudgalya S, Regnault N, Bernevig BA. 2018. Phys. Rev. B 98(23):235156
- 17. Schecter M, Iadecola T. 2019. Phys. Rev. Lett. 123(14):147201
- 18. Iadecola T, Schecter M. 2020. Phys. Rev. B 101(2):024306
- 19. Mark DK, Lin CJ, Motrunich OI. 2020. Phys. Rev. B 101(19):195131
- 20. Mark DK, Motrunich OI. 2020. Phys. Rev. B 102(7):075132
- 21. Moudgalya S, Regnault N, Bernevig BA. 2020. Phys. Rev. B 102(8):085140
- 22. Chattopadhyay S, Pichler H, Lukin MD, Ho WW. 2020. Phys. Rev. B 101(17):174308
- 23. O'Dea N, Burnell F, Chandran A, Khemani V. 2020. Phys. Rev. Res. 2(4):043305
- 24. Pakrouski K, Pallegar PN, Popov FK, Klebanov IR. 2020. Phys. Rev. Lett. 125(23):230602
- 25. Pakrouski K, Pallegar PN, Popov FK, Klebanov IR. 2021. Phys. Rev. Res. 3(4):043156
- 26. Ren J, Liang C, Fang C. 2021. Phys. Rev. Lett. 126(12):120604
- 27. Tang LH, O'Dea N, Chandran A. 2021. arXiv:2110.11448
- 28. Langlett CM, Yang ZC, Wildeboer J, Gorshkov AV, Iadecola T, Xu S. 2022. Phys. Rev. B 105(6):L060301
- 29. Omiya K, Müller M. 2022. arXiv:2203.00658
- 30. Houck AA, Türeci HE, Koch J. 2012. Nat. Phys. 8(4):292-99
- 31. Langen T, Geiger R, Schmiedmayer J. 2015. Annu. Rev. Condens. Matter Phys. 6:201-17
- 32. Morgado M, Whitlock S. 2021. AVS Quantum Sci. 3(2):023501
- 33. Monroe C, Campbell WC, Duan LM, Gong ZX, Gorshkov AV, et al. 2021. Rev. Mod. Phys. 93(2):025001
- 34. D'Alessio L, Kafri Y, Polkovnikov A, Rigol M. 2016. Adv. Phys. 65(3):239–362
- 35. Deutsch JM. 2018. Rep. Prog. Phys. 81(8):082001
- 36. Jensen RV, Shankar R. 1985. Phys. Rev. Lett. 54:1879-82
- 37. Deutsch JM. 1991. Phys. Rev. A 43(4):2046-49
- 38. Srednicki M. 1994. Phys. Rev. E 50(2):888-901
- 39. Rigol M, Dunjko V, Olshanii M. 2008. Nature 452:854–58
- 40. Vidmar L, Rigol M. 2016. 7. Stat. Mech. Theory Exp. 2016(6):064007
- 41. Santos LF. 2004. J. Phys. A Math. Gen. 37(17):4723-29
- 42. Rabson DA, Narozhny BN, Millis AJ. 2004. Phys. Rev. B 69(5):054403
- 43. Santos LF, Rigol M. 2010. Phys. Rev. E 81:036206
- 44. Modak R, Mukerjee S, Ramaswamy S. 2014. Phys. Rev. B 90(7):075152
- 45. Pandey M, Claeys PW, Campbell DK, Polkovnikov A, Sels D. 2020. Phys. Rev. X 10:041017
- 46. Nandkishore R, Huse DA. 2015. Annu. Rev. Condens. Matter Phys. 6:15–38
- 47. Abanin DA, Altman E, Bloch I, Serbyn M. 2019. Rev. Mod. Phys. 91(2):021001
- 48. Serbyn M, Papić Z, Abanin DA. 2013. Phys. Rev. Lett. 111(12):127201
- 49. Huse DA, Nandkishore R, Oganesyan V. 2014. Phys. Rev. B 90(17):174202
- 50. Swingle B. 2013. arXiv:1307.0507

- 51. Šuntajs J, Bonča J, Prosen T, Vidmar L. 2020. Phys. Rev. E 102(6):062144
- 52. Sels D, Polkovnikov A. 2021. Phys. Rev. E 104(5):054105
- 53. Abanin D, Bardarson J, De Tomasi G, Gopalakrishnan S, Khemani V, et al. 2021. Ann. Phys. 427:168415
- 54. Panda RK, Scardicchio A, Schulz M, Taylor SR, Žnidarič M. 2020. Europhys. Lett. 128(6):67003
- 55. Crowley PJD, Chandran A. 2022. SciPost Phys. 12:201
- 56. Morningstar A, Colmenarez L, Khemani V, Luitz DJ, Huse DA. 2022. Phys. Rev. B 105:174205
- 57. Serbyn M, Abanin DA, Papić Z. 2021. Nat. Phys. 17(6):675-85
- 58. Moudgalya S, Bernevig BA, Regnault N. 2022. Rep. Prog. Phys. 85:086501
- 59. Bernien H, Schwartz S, Keesling A, Levine H, Omran A, et al. 2017. Nature 551(7682):579-84
- 60. Affleck I, Kennedy T, Lieb EH, Tasaki H. 1987. Phys. Rev. Lett. 59(7):799-802
- 61. Mehta ML. 2004. Random Matrices. Amsterdam: Elsevier
- 62. Page DN. 1993. Phys. Rev. Lett. 71(9):1291-94
- 63. Yang CN. 1962. Rev. Mod. Phys. 34(4):694-704
- 64. Gorin T, Prosen T, Seligman TH, Žnidarič M. 2006. Phys. Rep. 435(2):33–156
- 65. Goussev A, Jalabert RA, Pastawski HM, Wisniacki DA. 2016. Philos. Trans. R. Soc. A 374:20150383
- 66. Choi S, Turner CJ, Pichler H, Ho WW, Michailidis AA, et al. 2019. Phys. Rev. Lett. 122(22):220603
- 67. Kitazawa A, Hijii K, Nomura K. 2003. J. Phys. A 36(23):L351-57
- 68. Ren J, Liang C, Fang C. 2022. Phys. Rev. Res. 4:013155
- 69. Vafek O, Regnault N, Bernevig BA. 2017. SciPost Phys. 3(6):043
- 70. van Voorden B, Minář J, Schoutens K. 2020. Phys. Rev. B 101:220305
- 71. Martin I, Matveev KA. 2022. Phys. Rev. B 105:045119
- 72. Schindler F, Regnault N, Bernevig BA. 2022. Phys. Rev. B 105(3):035146
- 73. Buča B, Tindall J, Jaksch D. 2019. Nat. Commun. 10:1730
- 74. Buča B, Purkayastha A, Guarnieri G, Mitchison MT, Jaksch D, Goold J. 2020. arXiv:2008.11166
- 75. Buča B. 2022. Phys. Rev. Lett. 128(10):100601
- 76. Moudgalya S, O'Brien E, Bernevig BA, Fendley P, Regnault N. 2020. Phys. Rev. B 102(8):085120
- 77. Khemani V, Laumann CR, Chandran A. 2019. Phys. Rev. B 99(16):161101
- 78. Kao W, Li K-Y, Lin K-Y, Gopalakrishnan S, Lev BL. 2021. *Science* 371(6526):296–300
- 79. Shibata N, Yoshioka N, Katsura H. 2020. Phys. Rev. Lett. 124(18):180604
- 80. Medenjak M, Buča B, Jaksch D. 2020. Phys. Rev. B 102(4):041117
- 81. Zhang Z, Mussardo G. 2022. Phys. Rev. B 106:134420
- 82. Qi XL, Ranard D. 2019. Quantum 3:159
- 83. Sattath O, Morampudi SC, Laumann CR, Moessner R. 2016. PNAS 113(23):6433-37
- 84. James AJA, Konik RM, Robinson NJ. 2019. Phys. Rev. Lett. 122(13):130603
- 85. Robinson NJ, James AJA, Konik RM. 2019. Phys. Rev. B 99(19):195108
- 86. Shastry B, Sutherland B. 1981. Physica 108B:1069-70
- 87. Chayes JT, Chayes L, Kivelson SA. 1989. Commun. Math. Phys. 123:53-83
- 88. Rokhsar DS, Kivelson SA. 1988. Phys. Rev. Lett. 61(20):2376-79
- 89. Castelnovo C, Chamon C, Mudry C, Pujol P. 2005. Ann. Phys. 318(2):316-44
- 90. Kitaev A. 2003. Ann. Phys. 303:2-30
- 91. Fannes M, Nachtergaele B, Werner RF. 1992. Commun. Math. Phys. 144(3):443-90
- 92. Nachtergaele B. 1996. Commun. Math. Phys. 175(3):565-606
- 93. Perez-Garcia D, Verstraete F, Wolf MM, Cirac JI. 2007. Quantum Inf. Comput. 7(5):401-30
- Fernández-González C, Schuch N, Wolf MM, Cirac JI, Pérez-García D. 2015. Commun. Math. Phys. 333:299–333
- 95. Shiraishi N, Mori T. 2017. Phys. Rev. Lett. 119(3):030601
- 96. Mori T, Shiraishi N. 2017. Phys. Rev. E 96(2):022153
- 97. Mondaini R, Mallavya K, Santos LF, Rigol M. 2018. Phys. Rev. Lett. 121(3):038901
- 98. McClarty PA, Haque M, Sen A, Richter J. 2020. Phys. Rev. B 102(22):224303
- 99. Kuno Y, Mizoguchi T, Hatsugai Y. 2020. Phys. Rev. B 102(24):241115
- 100. Banerjee D, Sen A. 2021. Phys. Rev. Lett. 126(22):220601
- 101. Biswas S, Banerjee D, Sen A. 2022. SciPost Phys. 12:148

- 102. Ok S, Choo K, Mudry C, Castelnovo C, Chamon C, Neupert T. 2019. Phys. Rev. Res. 1(3):033144
- 103. Srivatsa NS, Wildeboer J, Seidel A, Nielsen AEB. 2020. Phys. Rev. B 102(23):235106
- 104. Wildeboer J, Seidel A, Srivatsa NS, Nielsen AEB, Erten O. 2021. Phys. Rev. B 104(12):L121103
- 105. Lee K, Melendrez R, Pal A, Changlani HJ. 2020. Phys. Rev. B 101(24):241111
- 106. Khemani V, Hermele M, Nandkishore R. 2020. Phys. Rev. B 101(17):174204
- 107. Sala P, Rakovszky T, Verresen R, Knap M, Pollmann F. 2020. Phys. Rev. X 10:011047
- Moudgalya S, Prem A, Nandkishore R, Regnault N, Bernevig BA. 2021. In Memorial Volume for Shoucheng Zhang, ed. B Lian, C-X Liu, E Demler, S Kivelson, X-L Qi, pp. 147–209. Singapore: World Sci.
- 109. Yang ZC, Liu F, Gorshkov AV, Iadecola T. 2020. Phys. Rev. Lett. 124(20):207602
- 110. Rakovszky T, Sala P, Verresen R, Knap M, Pollmann F. 2020. Phys. Rev. B 101(12):125126
- 111. Moudgalya S, Motrunich OI. 2022. Phys. Rev. X 12:011050
- 112. Pai S, Pretko M. 2019. Phys. Rev. Lett. 123(13):136401
- 113. Nandkishore RM, Hermele M. 2019. Annu. Rev. Condens. Matter Phys. 10:295-313
- 114. Pretko M, Chen X, You Y. 2020. Int. J. Mod. Phys. A 35(6):2030003
- 115. Tao R, Thouless DJ. 1983. Phys. Rev. B 28(2):1142-44
- 116. Bergholtz EJ, Karlhede A. 2006. J. Stat. Mech. Theory Exp. 2006(04):L04001
- 17. Moudgalya S, Bernevig BA, Regnault N. 2020. Phys. Rev. B 102(19):195150
- 118. Abanin D, De Roeck W, Ho WW, Huveneers F. 2017. Commun. Math. Phys. 354(3):809-27
- 119. Mori T, Kuwahara T, Saito K. 2016. Phys. Rev. Lett. 116(12):120401
- 120. Guo Q, Cheng C, Li H, Xu S, Zhang P, et al. 2021. Phys. Rev. Lett. 127(24):240502
- 121. Wang YY, Sun ZH, Fan H. 2021. Phys. Rev. B 104(20):205122
- 122. Morong W, Liu F, Becker P, Collins KS, Feng L, et al. 2021. Nature 599(7885):393-98
- 123. Schulz M, Hooley CA, Moessner R, Pollmann F. 2019. Phys. Rev. Lett. 122(4):040606
- 124. van Nieuwenburg E, Baum Y, Refael G. 2019. PNAS 116(19):9269-74
- 125. Gromov A, Lucas A, Nandkishore RM. 2020. Phys. Rev. Res. 2(3):033124
- 126. Grosvenor KT, Hoyos C, Peña Benitez F, Surówka P. 2021. Phys. Rev. Res. 3(4):043186
- 127. Iaconis J, Lucas A, Nandkishore R. 2021. Phys. Rev. E 103(2):022142
- 128. Iadecola T, Žnidarič M. 2019. Phys. Rev. Lett. 123(3):036403
- 129. De Tomasi G, Hetterich D, Sala P, Pollmann F. 2019. Phys. Rev. B 100(21):214313
- 130. Nachtergaele B, Warzel S, Young A. 2020. J. Phys. A Math. Theor. 54:01LT01
- 131. Lan Z, van Horssen M, Powell S, Garrahan JP. 2018. Phys. Rev. Lett. 121(4):040603
- 132. Olmos B, Müller M, Lesanovsky I. 2010. New J. Phys. 12:013024
- 133. Gopalakrishnan S, Zakirov B. 2018. Quantum Sci. Technol. 3(4):044004
- 134. Gopalakrishnan S. 2018. Phys. Rev. B 98(6):060302
- 135. Hudomal A, Vasić I, Regnault N, Papić Z. 2020. Commun. Phys. 3:99
- 136. Zhao H, Vovrosh J, Mintert F, Knolle J. 2020. Phys. Rev. Lett. 124(16):160604
- 137. Zhao H, Smith A, Mintert F, Knolle J. 2021. Phys. Rev. Lett. 127(15):150601
- 138. Sikora O, Shannon N, Pollmann F, Penc K, Fulde P. 2011. Phys. Rev. B 84(11):115129
- 139. Zhang Z, Røising HS. 2022. arXiv:2206.01758
- 140. Moessner R, Sondhi SL. 2001. Phys. Rev. Lett. 86(9):1881-84
- 141. Cépas O, Akhmetiev PM. 2021. SciPost Phys. 10(2):42
- 142. Yin H, Chakraborty B. 2001. Phys. Rev. Lett. 86(10):2058-61
- 143. Garrahan JP, Chandler D. 2002. Phys. Rev. Lett. 89(3):035704
- 144. Garrahan JP, Jack RL, Lecomte V, Pitard E, van Duijvendijk K, van Wijland F. 2007. Phys. Rev. Lett. 98(19):195702
- 145. van Horssen M, Levi E, Garrahan JP. 2015. Phys. Rev. B 92(10):100305
- 146. Pancotti N, Giudice G, Cirac JI, Garrahan JP, Bañuls MC. 2020. Phys. Rev. X 10(2):021051
- Charbonneau P, Kurchan J, Parisi G, Urbani P, Zamponi F. 2017. Annu. Rev. Condens. Matter Phys. 8:265–88
- 148. Bluvstein D, Omran A, Levine H, Keesling A, Semeghini G, et al. 2021. Science 371(6536):1355-59
- 149. Jaksch D, Cirac JI, Zoller P, Rolston SL, Côté R, Lukin MD. 2000. Phys. Rev. Lett. 85(10):2208–11
- 150. Fendley P, Sengupta K, Sachdev S. 2004. Phys. Rev. B 69(7):075106

- 151. Surace FM, Mazza PP, Giudici G, Lerose A, Gambassi A, Dalmonte M. 2020. Phys. Rev. X 10(2):021041
- 152. Moessner R, Sondhi SL. 2001. Phys. Rev. B 63(22):224401
- 153. Laumann CR, Moessner R, Scardicchio A, Sondhi SL. 2012. Phys. Rev. Lett. 109(3):030502
- 154. Chen C, Burnell F, Chandran A. 2018. Phys. Rev. Lett. 121(8):085701
- 155. Gutzwiller MC. 1963. Phys. Rev. Lett. 10(5):159-62
- 156. Anderson PW. 1987. Science 235:1196-98
- 157. Castelnovo C, Moessner R, Sondhi S. 2012. Annu. Rev. Condens. Matter Phys. 3:35-55
- Girvin SM. 1999. In Topological Aspects of Low Dimensional Systems, Vol. 69, ed. A Comtet, T Jolicoeur, S Ouvry, F David, pp. 53–175. Berlin: Springer
- 159. Turner CJ, Michailidis AA, Abanin DA, Serbyn M, Papić Z. 2018. Phys. Rev. B 98(15):155134
- 160. Desaules JY, Bull K, Daniel A, Papić Z. 2022. Phys. Rev. B 105:245137
- 161. Turner CJ, Desaules JY, Bull K, Papić Z. 2021. Phys. Rev. X 11(2):021021
- 162. Ho WW, Choi S, Pichler H, Lukin MD. 2019. Phys. Rev. Lett. 122(4):040603
- 163. Michailidis AA, Turner CJ, Papić Z, Abanin DA, Serbyn M. 2020. Phys. Rev. Res. 2(2):022065
- 164. Michailidis AA, Turner CJ, Papić Z, Abanin DA, Serbyn M. 2020. Phys. Rev. X 10:011055
- 165. Haegeman J, Cirac JI, Osborne TJ, Pižorn I, Verschelde H, Verstraete F. 2011. Phys. Rev. Lett. 107(7):070601
- 166. Franchini F. 2017. Lecture Notes in Physics, Vol. 940: An Introduction to Integrable Techniques for One-Dimensional Quantum Systems. Cham: Springer. 1st ed.
- 167. Berges J, Borsányi S, Wetterich C. 2004. Phys. Rev. Lett. 93(14):142002
- 168. Kinoshita T, Wenger T, Weiss DS. 2006. Nature 440(7086):900-903
- 169. Gring M, Kuhnert M, Langen T, Kitagawa T, Rauer B, et al. 2012. Science 337(6100):1318-22
- 170. Neyenhuis B, Zhang J, Hess PW, Smith J, Lee AC, et al. 2017. Sci. Adv. 3(8):e1700672
- 171. Eckstein M, Hackl A, Kehrein S, Kollar M, Moeckel M, et al. 2009. Eur. Phys. J. Spec. Top. 180:217-35
- 172. Eisert J, Friesdorf M, Gogolin C. 2015. Nat. Phys. 11(2):124-30
- 173. Vasseur R, Moore JE. 2016. J. Stat. Mech. Theory Exp. 2016(6):064010
- 174. Windt B, Pichler H. 2022. Phys. Rev. Lett. 128(9):090606
- 175. Iadecola T, Schecter M, Xu S. 2019. Phys. Rev. B 100(18):184312
- 176. Ovchinnikov AA, Dmitriev DV, Krivnov VY, Cheranovskii VO. 2003. Phys. Rev. B 68(21):214406
- 177. Chen IC, Burdick B, Yao Y, Orth PP, Iadecola T. 2022. Phys. Rev. Res. 4:043027
- 178. Pan L, Zhai H. 2022. Phys. Rev. Res 4:L032037
- 179. Lesanovsky I. 2012. Phys. Rev. Lett. 108(10):105301
- 180. Lin CJ, Motrunich OI. 2019. Phys. Rev. Lett. 122(17):173401
- 181. Schecter M, Iadecola T. 2018. Phys. Rev. B 98(3):035139
- 182. Bull K, Desaules JY, Papić Z. 2020. Phys. Rev. B 101(16):165139
- 183. Su GX, Sun H, Hudomal A, Desaules JY, Zhou ZY, et al. 2022. arXiv:2201.00821
- Zhang P, Dong H, Gao Y, Zhao L, Hao J, et al. 2022. Nat. Phys. 2022: https://doi.org/10.1038/s41567-022-01784-9
- 185. Cazalilla MA, Citro R, Giamarchi T, Orignac E, Rigol M. 2011. Rev. Mod. Phys. 83:1405–66
- 186. Lin CJ, Chandran A, Motrunich OI. 2020. Phys. Rev. Res. 2(3):033044
- 187. Mondragon-Shem I, Vavilov MG, Martin I. 2021. PRX Quantum 2(3):030349
- 188. Lazarides A, Das A, Moessner R. 2014. Phys. Rev. E 90:012110
- 189. D'Alessio L, Rigol M. 2014. Phys. Rev. X 4(4):041048
- 190. Haldar A, Sen D, Moessner R, Das A. 2021. Phys. Rev. X 11(2):021008
- 191. Mukherjee B, Nandy S, Sen A, Sen D, Sengupta K. 2020. Phys. Rev. B 101(24):245107
- 192. Mizuta K, Takasan K, Kawakami N. 2020. Phys. Rev. Res. 2(3):033284
- 193. Sugiura S, Kuwahara T, Saito K. 2021. Phys. Rev. Res. 3:L012010
- 194. Maskara N, Michailidis AA, Ho WW, Bluvstein D, Choi S, et al. 2021. Phys. Rev. Lett. 127(9):090602
- 195. Iadecola T, Vijay S. 2020. Phys. Rev. B 102(18):180302
- 196. Wilkinson JWP, Klobas K, Prosen T, Garrahan JP. 2020. Phys. Rev. E 102(6):062107
- 197. Rozon PG, Gullans MJ, Agarwal K. 2021. arXiv:2112.12153
- 198. Khemani V, Lazarides A, Moessner R, Sondhi SL. 2016. Phys. Rev. Lett. 116(25):250401

- 199. Sacha K, Zakrzewski J. 2017. Rep. Prog. Phys. 81:016401
- 200. Khemani V, Moessner R, Sondhi SL. 2019. arXiv:1910.10745
- 201. Else DV, Monroe C, Nayak C, Yao NY. 2020. Annu. Rev. Condens. Matter Phys. 11:467-99
- 202. Wisniacki D, Carlo GG. 2008. Phys. Rev. E 77(4):045201
- 203. Srivatsa NS, Moessner R, Nielsen AEB. 2020. Phys. Rev. Lett. 125(24):240401
- 204. Jepsen PN, Lee YK, Lin H, Dimitrova I, Margalit Y, et al. 2022. Nat. Phys. 18:899-904
- 205. Dooley S. 2021. PRX Quantum 2(2):020330
- 206. Desaules JY, Pietracaprina F, Papić Z, Goold J, Pappalardi S. 2022. Phys. Rev. Lett. 129:020601



Contents

Annual Review of Condensed Matter Physics

Volume 14, 2023

A Journey Through Nonlinear Dynamics: The Case of Temperature Gradients Albert Libchaber
An Adventure into the World of Soft Matter Dominique Langevin
Floquet States in Open Quantum Systems Takashi Mori
Generalized Symmetries in Condensed Matter John McGreevy
Non-Hermitian Topological Phenomena: A Review Nobuyuki Okuma and Masatoshi Sato
Modeling Active Colloids: From Active Brownian Particles to Hydrodynamic and Chemical Fields Andreas Zöttl and Holger Stark
Spin Seebeck Effect: Sensitive Probe for Elementary Excitation, Spin Correlation, Transport, Magnetic Order, and Domains in Solids Takashi Kikkawa and Eiji Saitoh
Superconductivity and Local Inversion-Symmetry Breaking Mark H. Fischer, Manfred Sigrist, Daniel F. Agterberg, and Youichi Yanase
Tensor Network Algorithms: A Route Map Mari Carmen Bañuls
Spatial and Temporal Organization of Chromatin at Small and Large Scales Helmut Schiessel
Dissecting Flux Balances to Measure Energetic Costs in Cell Biology: Techniques and Challenges Easun Arunachalam, William Ireland, Xingbo Yang, and Daniel Needleman
Data-Driven Discovery of Robust Materials for Photocatalytic Energy Conversion Arunima K. Singh, Rachel Gorelik, and Tathagata Biswas

A. Alexandradinata and Leonid Glazman	261
Physics of Human Crowds Alessandro Corbetta and Federico Toschi	311
Random Quantum Circuits Matthew P.A. Fisher, Vedika Khemani, Adam Nahum, and Sagar Vijay	335
Swimming in Complex Fluids Saverio E. Spagnolie and Patrick T. Underhill	381
Learning Without Neurons in Physical Systems Menachem Stern and Arvind Murugan	417
Quantum Many-Body Scars: A Quasiparticle Perspective Anushya Chandran, Thomas Iadecola, Vedika Khemani, and Roderich Moessner	443
Odd Viscosity and Odd Elasticity Michel Fruchart, Colin Scheibner, and Vincenzo Vitelli	471

Errata

An online log of corrections to *Annual Review of Condensed Matter Physics* articles may be found at http://www.annualreviews.org/errata/conmatphys